Heritage Science

RESEARCH

Open Access

ZnO, TiO_2 and Fe_3O_4/Carbopol hybrid nanogels for the cleaner process of paper manuscripts from dust stains and soil remains

Rushdya Rabee Ali Hassan[1*], Haidi M. Hassan[1], Yassmine A. Mohamed[1], Mai E. M. Ismail[1], Yara Farid[1], Hager Mohamed[1], Sameh H. Ismail[2], Mohamed Z. M. Salem[3*] and Mostafa Abdel-Hamied[1*]

Abstract

There are many paper manuscripts at museums, stores, and libraries that have different stains. The dust stains and soil remains played an important role in the degradation of these manuscripts. Therefore, the cleaning process for these stains is important to process. Unfortunately, the removal of stains by some traditional techniques can be hazardous to the paper's fibers. Therefore, this study aims to evaluate innovative nanoparticle gels in the cleaning process of dust stains from paper manuscripts. The synthesized nanomaterials [Fe_3O_4, TiO_2, and ZnO]/Carbopol hybrid nanogel were examined in order to investigate the surface morphology, determine the physio-chemical properties, for phase structure, using scanning electron microscope (SEM), transmission electron microscope (TEM), AFM, DLS, XRD, and Zeta potential. Some stained paper samples were prepared and exposed to accelerated thermal aging at 100 °C for 72 h. The evaluation of the cleaning by nanogel was performed by different analytical procedures containing investigation with a USB digital microscope, SEM, color change, mechanical properties, and ATR-FTIR analysis. The results of this study showed that ZnO/Carbopol hybrid nanogel at high viscosity gave the best results in the cleaning process of mud stains through the ability to dismantle mud particles and increase surface contact with the solvent. The aged treated sample with high viscosity form of ZnO NPs/carbopol hybrid nanogel gave the highest tensile strength value of (56.0 N). The treated samples with the high viscosity form of ZnO NPs/carbopol hybrid nanogel gave the highest value of elongation (1.398%) before aging. It also does not affect the chemical composition of the paper after cleaning it, but rather on the whole, it bites the hydration of the paper, which positively affects the properties of the treated paper.

Keywords Paper conservation, Gel cleaning, Hybrid nanogel, Magnetite, Rutile, Zincite

Introduction

There are many paper manuscripts housed in different stores, libraries, and museums are suffered from numerous kinds of stains resulting from different deterioration factors [1–4], especially dust stains and soil remains. A lot of pages of the manuscripts are extremely cockled which leads to the ingress of dust inside the text block. The dust has a particular challenge for historical libraries [5–7]. Dirt and soil remain leads to different signs of damage to paper manuscripts like a scratchy action for the paper's fibers and lead to weakness of paper manuscripts [5, 8–10]. Dust and soil remains may become acidic due to

*Correspondence:
Rushdya Rabee Ali Hassan
rushdyarabii@cu.edu.eg
Mohamed Z. M. Salem
mohamed-salem@alexu.edu.eg
Mostafa Abdel-Hamied
mostafa_farag@cu.edu.eg
[1] Conservation Department, Faculty of Archaeology, Cairo University, Giza 12613, Egypt
[2] Faculty of Nanotechnology for Postgraduate Studies, Sheikh Zayed Campus, Cairo University, 6th October City, Giza 12588, Egypt
[3] Forestry and Wood Technology Department, Faculty of Agriculture (EL-Shatby), Alexandria University, Alexandria 21545, Egypt

the absorption of atmospheric pollutants such as sulfur dioxide from the surrounding environmental conditions [11–13]. The previous gas (SiO_2) in combination with moisture can react with the metal compounds (Iron) found on the surface of the paper manuscripts in dust form and converted to sulfuric acid which is absorbed by paper sheets and consequently, weakness of its mechanical properties and flexibility [14, 15].

Dust and soil remain found on the paper manuscript's surface and often contain mold spores, particularly in an uncontrolled environment. Additionally, the components of dust can provide a nutrient source for insects and microorganisms [14, 16]. The dust and soil remaining can absorb moisture from the surrounding environmental conditions which facilitate penetration of particulates of dust inside the paper sheets, consequently making it difficult to clean by the surface cleaning methods. The presence of surface dust leads to the staining of the paper sheets and reduces the artistic and historical values of paper manuscripts [17]. The removal of dust from the manuscripts, books, and other contents of libraries needs a high cost [18]. Cementation of dust occurred at high humidity, where calcium ions can leach from dust particles and redeposit forming microcrystalline calcite which cements the dust particle to the substrate and the hygroscopic feature of paper-enhanced cementation [19, 20], where at high humidity, dust adheres very successfully to paper manuscripts. Many of the bacteria present in these materials, and particularly in archive materials, grow using very low concentrations of nutrients and may cause chemical and esthetic biodeterioration, as well as facilitating the last development of other microorganisms such as fungi, which are well-known deteriogens [21]. Their initial growth on materials is usually due to other organic material present in the dust, not to the nutrients in the supports [22].

Due to the previous, the dust stains and soil remains must be removed and cleaned from paper manuscripts. The cleaning process is one of the most vital processes for the treatment of paper manuscripts [23, 24]. Unfortunately, some traditional methods such as solvents and chemical bleaching used for cleaning some stains lead to damage to the fibers of the treated paper [25] and most organic solvents (such as toluene) used in the treatment of paper manuscripts lead to degradation of the treated paper manuscripts, where these solvents led to an acceleration of oxidation and hydrolysis processes of paper [1].

One of the most important disciplines in cultural heritage conservation sciences these days is research into more effective, and stable time, new conservation treatments [26, 27]. The use of gel is considered one of the most important processes used for cleaning paper manuscripts because it is easy and securely controlled [1] and it does not need liquid treatments [28]. Accordingly, the gel of some nanoparticles (NPs) such as ZnO, TiO_2, and Fe_3O_4 gel have been evaluated for cleaning paper manuscripts in the present work. Out of our knowledge, gels contain ZnO NPs, TiO_2 NPs, and Fe_3O_4 NPs have never been applied in cleaning paper manuscripts prior to this study.

ZnO NPs were chosen in this study due to its advantages such as being affordable and having many active sites with high surface reactivity [29, 30]. ZnO NPs showed high absorption efficacy of light radiations, environmental safety, high homogeneity, relatively low process temperature and UV protection [31, 32] and antibacterial properties [33].

In nanoscale and microscale formulations, ZnO NPs are now being investigated as antibacterial agents [34]. When used in conjunction with components for biosensing and wound healing, ZnO NPs can trace minute amounts of biomarkers associated with different illnesses [35]. Additionally, it has been revealed that ZnO NPs may deliver and detect medicines [36]. ZnO NPs have superhydrophobicity, low electron conductivity, and excellent heat resistance [37, 38], which give it multifunction purpose in medical application [39].

Excellent reusable self-cleaning capabilities of ZnO NPs were demonstrated, and these capabilities are crucial for stain removal because they prevent dust or dirt accumulation on the treated surface [40, 41]. ZnO NPs give protection and preservation of paper works against deterioration factors and it uses as a protective coating on the surface of paper fibers [42]. When ZnO NPs were applied to the paper surface for the coating to improve the surface strength and softness [43–45] and protect paper from the damaging effects of UV light, air pollutants, and micro-organisms like fungi and bacteria [45, 46].

TiO_2 is a white non-combustible and odorless powder [47]. It is one of the most important inorganic minerals due to the potential applications of TiO_2 NPs in different fields, non-toxicity, stability and optical, and adsorption properties [47, 48]. Additionally, TiO_2 is super hydrophobic material [49]. TiO_2 NPs have been made using green, chemical, physical, and biological synthesis techniques. Green methods have been found to be more effective than chemical synthesis techniques because they use fewer precursors, use less time, and use less energy [50, 51].

Iron oxide nanoparticles (Fe_3O_4 NPs) are widely studied in various fields of research like magnetic resonance (MR) imaging applications [52], platforms for tumor imaging and therapy or improved and targeted cellular absorption by alterations to the surface layer coating [53], customized medication delivery and environmental cleanup [54] and antimicrobial bioactives [55, 56]. Fe_3O_4

NPs are frequently produced by chemical reduction, thermal breakdown, and hydrothermal synthesis techniques [54].

Therefore, the aim of this work was to evaluate the efficiency of nanogels containing, either ZnO NPs, TiO_2 NPs, or Fe_3O_4 NPs in the forms of low or high viscosity in the cleaning process of paper manuscripts.

Materials and methods

Preparation of stained paper samples

The paper samples which had been used in this study are Whatman filter paper (100% of pure cotton fibers)-GE Healthcare Life Sciences with the following technical information: CAT No. 1442–150, Model quantitative filter Whatman ashless, grade: 42, diameter: 150 mm. Whatman was purchased from Sigma company (Sigma–Aldrich, Mo, St. Louis, USA). From the field study by authors at the Center of Conservation of Antiquities, Egypt, it was noticed different paper manuscripts suffered from dust stains and soil remains (Fig. 1). The dust used in this study was collected by soft brush from a storehouse of the special library (Fig. 2), Cairo, Egypt.

The application of a dust layer on Whatman paper was performed according to Elnaggar et al. [57]. Briefly, the collected dust (Fig. 3A) was mixed with distilled water (Fig. 3B). The Whatman paper samples were covered with a thin layer of the prepared dust using a soft brush (Fig. 3C, D). The stained paper samples (Fig. 3E) were left to dry at room temperature (Fig. 3F). After staining, the samples were subjected to an aging process before carrying out the cleaning experiments.

Fig. 2 The storehouse of the special library, Cairo, Egypt, which the dust has been collected from it using a soft brush. Photos were taken by the co-author Mostafa Abdel-Hamied

Preparation of nanomaterials/carbopol hybrid nanogels

Chemicals

Hematite ore (Aswan mins), ammonia water (NH_4OH, 34%, El Naser Chemical Co., Egypt) Carbopol, Trimethylamine, TiO_2, Zn $(CH_3CO_2)_2{\cdot}2H_2O$, H_2O_2 and

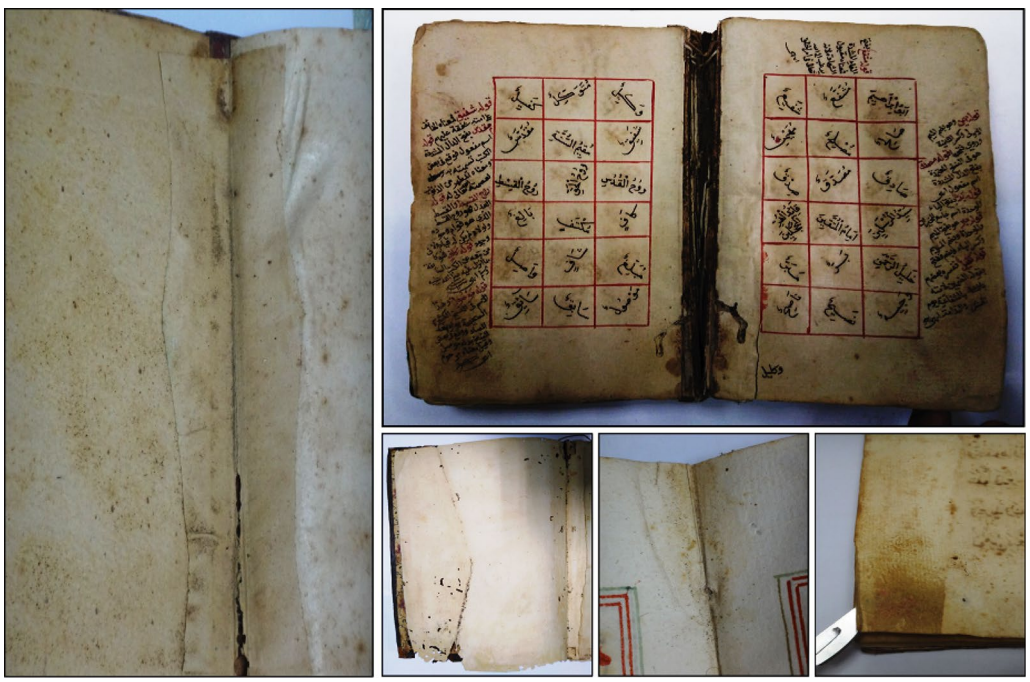

Fig. 1 Some examples of dust stains and soil remain on some paper manuscripts (From the field survey of researchers). Photos were taken by the co-author Mostafa Abdel-Hamied

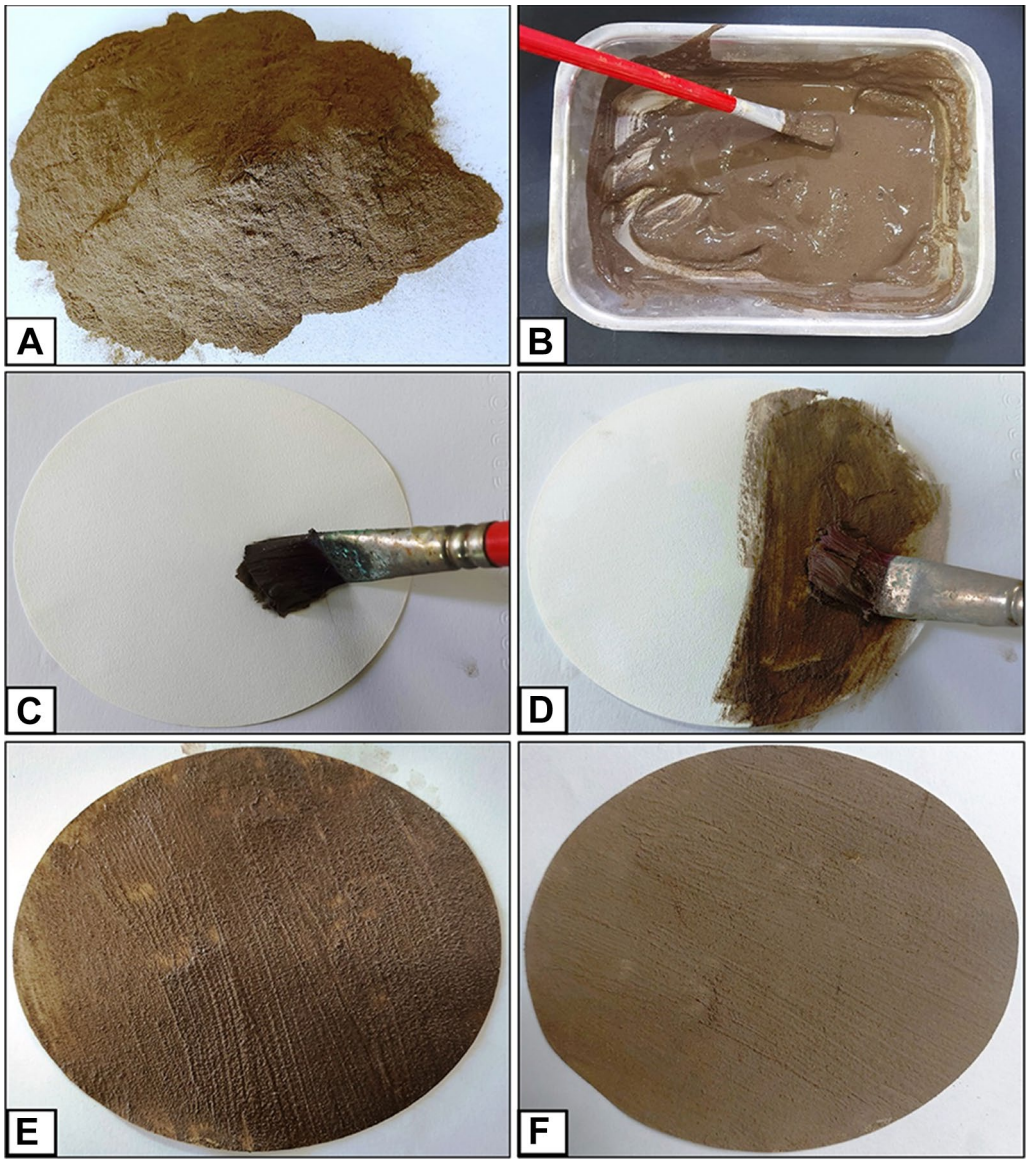

Fig. 3 Preparation steps of stained paper; **A** The collected dust; **B** The prepared dust mixed with distilled water; **C**, **D** Application of a thin layer of the prepared dust over the what-man paper by brush; **E** The stained paper before drying; **F** The stained paper after drying

NaOH (Sigma Chemical Co., India) were used without any purification with lab grade. The neutralization of carbopol hybrid nanogels produced the highest possible viscosity. At a pH between 6.0 and 7.0, the maximum viscosity is often attained. In this work, ammonia water (NH4OH, 34% added) was used to achieve a pH of 9.0, and as a result, the viscosity of carbopol hybrid nanogels started to drop to make them appropriate for application on the surface of paper.

Synthesis of ZnO NPs/carbopol hybrid nanogel

Zincite nanoparticles (ZnO NPs) were synthesized by the precipitation method according to Ismail et al. [58]. In a typical synthesis, zinc acetate dihydrate as source material and Ammonia solution 33% (NH_3 basis) in aqueous solution (NH_4OH) as a precipitating agent were used. The ZnO NPs were produced by dissolving the appropriate weight of zinc acetate in 200 ml of doubled deionized water to give 0.2 M Zn solution. Subsequently, the Zn solution was subjected to ultra-sonication radiation using Hielscher UP400S (400 W, 24 kHz, Hielscher Ultrasonics GmbH, Germany), at an amplitude of 80% and a cycle of 0.8 for 10 min at a temperature of 60 °C. At the same time of sonication, the ammonia solution was added dropwise to the Zn solution. When ZnO NPs started to form and develop, the ammonia solution addition continued until

all of the ZnO NPs had precipitated. Finally, the white precipitate was washed three times with doubled deionized water that had been doubled before being air-dried for 24 h.

The sonochemical method was used to synthesis a ZnO NPs/carbopol hybrid nanogel. 1 g of carbopol 940 was dissolved in 500 ml deionized water, added to washed ZnO NPs, and placed in a sonication prop device under the conditions of 90 amplitude and 90 cycles. Next, 100 ml of trimethylamine was added drop by drop with continuous sonication until white gel formation. To create a thicker ZnO NPs/carbopol hybrid nanogel, the last process with various amounts of carbopol and trimethylamine (2 g to 200 ml) was repeated. High and low-viscosity ZnO NPs/carbopol hybrid nanogels have been created.

Synthesis of TiO_2 NPs /carbopol hybrid nanogel

Firstly, the synthesis of rutile nanoparticles (TiO_2 NPs) by the sonochemical method was done according to Gharib et al. [59]. TiO_2 (0.5 g) was added to 100 ml of 10 M NaOH and then subjected to ultrasonication for 4 h at room temperature with continual stirring at 90% amplitude and 0.9 cycles. Then used three further washes of doubled deionized water to wash the final precipitate. One gram of Carbopol 940 dissolved in 500 ml deionized water was added to washed TiO_2 NPs and placed in a sonication prop device with the conditions of amplitude 90 and cycle 90%. Next, 100 ml of trimethyl-amine was added drop by drop with continuous sonication until white gel formation. This was done using a sonochemical method. To create a thicker TiO_2 NPs/carbopol hybrid nanogel, the last procedure was repeated with various concentrations of carbopol and trimethylamine (2 g to 200 mL). Both a high and low viscosity TiO_2 NPs/carbopol hybrid nanogel has been created.

Synthesis of Fe_3O_4 NPs/carbopol hybrid nanogel

Magnetite nanoparticles (Fe_3O_4 NPs) were synthesized using the method described by Hamdy et al. [60]. 0.3 g of the hematite ore was added to 30 mL of H_2O_2 drop by drop in the same time the mixture was subjected to ultrasound of 60 kHz for 2 h in an ultrasonic device (Sonica 4200 EPS3, Italy) until the black particles of Fe_3O_4 was obtained. After 0.5 h, the Fe_3O_4 NPs (blackly colored) had precipitated from the supernatant (reddishly colored). The Fe_3O_4 NPs had been separated from the solution by centrifugation at 4000 RPM and finally, the Fe_3O_4 NPs have washed four times using methanol. In a typical synthesis of Fe_3O_4 NPs/carbopol hybrid nanogel, 0.1 g of Fe_3O_4 NPs desperation in 50 ml of ethanol is added to a solution of 0.5 g carbopol dissolved in 50 ml ethanol and stir the mixture using a mechanical stirrer for 45 min. Next, 0.5 ml of Trimethylamine was added drop by drop and stirred for another 30 min until obtaining black gel. Fe_3O_4 NPs/carbopol hybrid nanogel has been prepared in high and low-viscosity.

Application of nanomaterials/carbopol hybrid nanogels

Firstly, some mechanical tools such as soft brushes, and scalpels have been used in order to remove loose particulates. Followed by, the application of the nanomaterials/carbopol hybrid nanogels. The application of the prepared high-viscosity of nanogels was performed by spatula (Fig. 4A), then covered with a polyethylene sheet (Fig. 4B, C) and left in order to react with the dust stain layer. After approximately 10 min, the nanogel layer was removed using a spatula (Fig. 4D), and the residue was removed with a cotton swab (Fig. 4E). On the other hand, the low viscosity from the prepared nanogels was applied using a soft brush (Fig. 4F, G) [61, 62] and the cleaning process was achieved by the cotton swab (Fig. 4H).

Accelerated thermal ageing for the stained and cleaned paper samples

The dried stained paper samples were aged for six days at 105 °C, which is chosen to be the equivalent of 50 years of natural aging [63]. After being cleaned, the test paper samples underwent 27 days of thermal aging at 105 °C [28, 64].

Analytical methods used

For the investigation of produced nanomaterials (Fe_3O_4, TiO_2, and ZnO)/Carbopol hybrid nanogel and for the assessment of the cleaning procedure for paper samples, a variety of analytical techniques have been applied.

Transmission electron microscope (TEM)

High-resolution Transmission Electron Microscope (JEOL TEM-2100, Japan) was used to supply the texture of the synthesized nanomaterials/Carbopol hybrid nanogel [65, 66]. Before testing, samples were thoroughly suspended and sonicated with an ultrasonic prop. After that, 50 µm of slurry was placed into a TEM grid, and measurements were made under 200 kV conditions.

Atomic force microscope (AFM)

Topographic images with 2D and 3D surfaces were obtained by Atomic Force Microscope (AFM, 5600LS, Agilent, USA) at the Faculty of Nanotechnology, Cairo University, Giza, Egypt. Firstly, the sample was suspended, and thoroughly sonicated with an ultrasonic generator, and then 100 µm of the slurry was placed on a mica plate for measurement using the contact mode. Al tip and study region are 100 nm × 100 nm.

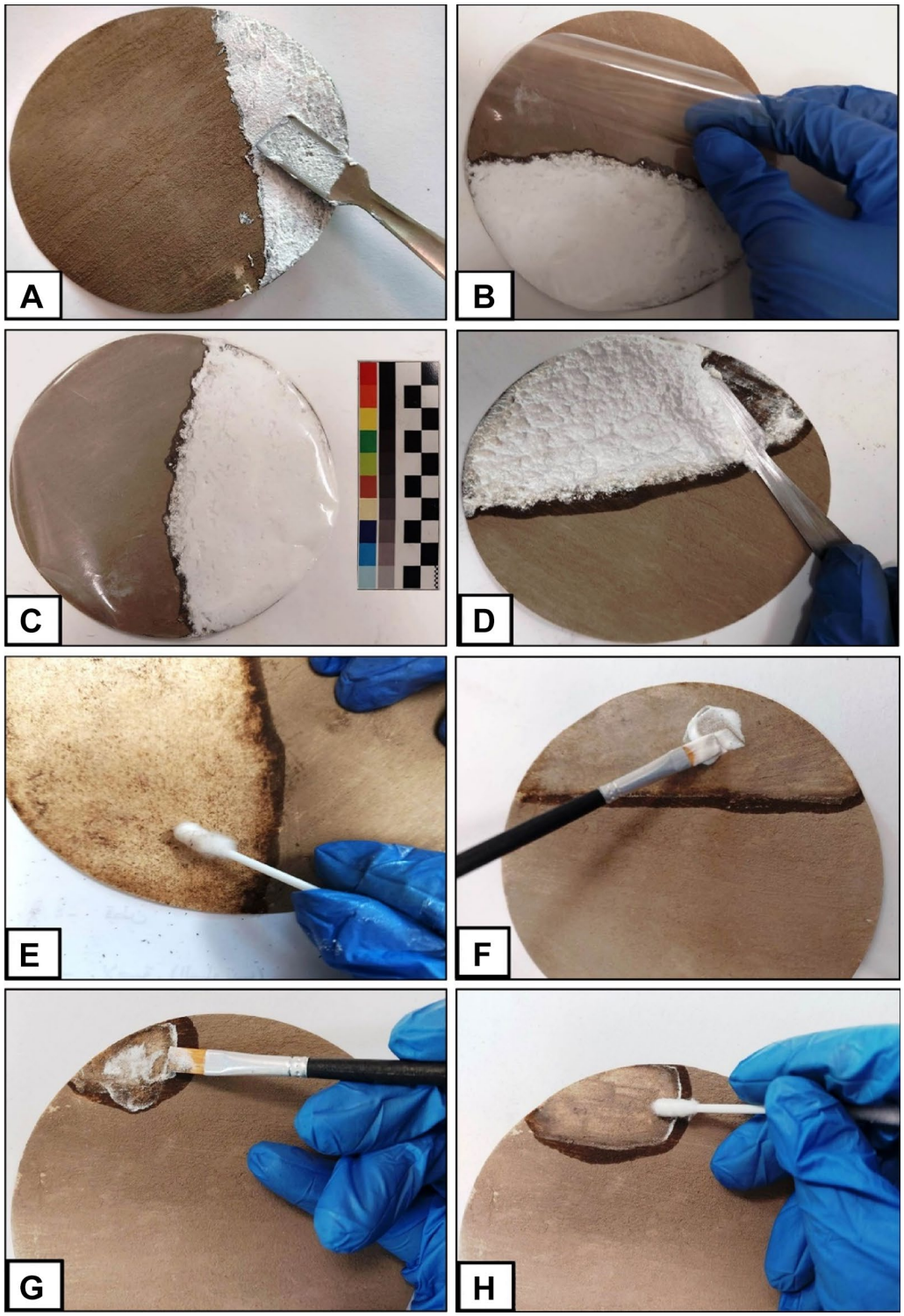

Fig. 4 Application and cleaning process using the high and low viscosity of nanogels; **A** Application of high viscosity nanogel by spatula; **B**, **C** Covering the applied high viscosity gel with polyethylene sheet; **D** Removing the applied layer using a spatula; **E** Removing the residue with a cotton swab; **F**, **G** Application of the low viscosity from nanogels using a soft brush; **H** Cleaning process by a cotton swab

X-Ray diffraction (XRD)

A non-destructive analytical method used to ascertain the crystallographic structure of materials is X-ray diffraction (XRD, Philips, PAN analytical X'Pert, CuKα radiation, USA) at the Faculty of Nanotechnology, Cairo University, Egypt was used to analyze the synthesized nanomaterials/Carbopol hybrid nanogel. XRD includes shining an X-ray beam on the sample and analyzing the diffraction pattern that results. The crystal structure, lattice spacing, and atom orientation of the sample are all revealed by the diffraction pattern. The materials were first dried, ground into a powder, and then placed in an X-ray diffractometer for measurement at a 2-theta range of 5 to 80° under conditions of 30 mA and 10 kV.

Zeta potential

The electrokinetic potential of particles in solution is measured by the zeta potential. The stability of colloidal suspensions can be assessed using the zeta potential, which also offers details on the surface charges of the particles and their interactions with one another. Zeta potential was performed by a Zeta analyzer device manufactured by Malvern Instruments Ltd. (Nano Sight NS500, USA). Prior to testing, samples were suspended and thoroughly sonicated using an ultrasonic prop. Then, 1000 µm of slurry containing two Ag electrodes was placed into a quartz zeta potential cuvette for measurement under constant current and 25 °C temperature conditions.

Dynamic light scattering (DLS)

The measurement and size distribution of the synthesized nanomaterials/Carbopol hybrid nanogel was achieved by a dynamic light scattering (DLS) device manufactured by Malvern Instruments Ltd. (Nano Sight NS500, USA). DLS is a method for calculating the variations in scattered light based on the Brownian motion of particles. DLS can offer details on the hydrodynamic diameter and particle size distribution of particles in solution. Before testing, samples were suspended and thoroughly sonicated using an ultrasonic generator. Then, 1000 µm of the slurry was placed into a DLS rounded quartz cuvette coated with $BaCl_2$, and the temperature was set at 25 °C for measurements condition.

Scanning electron microscope (SEM)

A beam of electrons is used in the scanning electron microscope (SEM) method to scan a sample's surface and generate high-resolution images. SEM offers details on the composition, elemental analysis, and topography of the sample. A field emission scanning electron microscopy (FESEM, JSM-6701F Plus, JEOL, Japan) was used to investigate the surface morphology of the synthesized nanomaterials/carbopol hybrid nanogel. Additionally, Zeiss LEO 1550 (SEM LEO 1550VP; Carl Zeiss AG, Oberkochen, Germany), equipped with an Edwards Scan Coat K550X sputter coater (Gordon Brothers, Boston, MA, USA) at Asyut University was used to investigate the surface morphology for stained and cleaned paper samples. The sample size was not exceed 10 cm^2, and the thickness was less than 10 mm. For the purpose of obtaining more precise images, several scans were performed at various magnifications.

Digital microscope (USB microscope)

The USB digital microscope (model PZ01; Shenzhen Super Eyes Co., Ltd., Guangdong, China) was used for the investigation of the surface of the experimental paper samples with magnification from 200-500X.

Color change by spectrophotometer

The color change of the non-cleaned and cleaned paper samples was performed with a spectrophotometer: Optimatch 3100 (Model No. CE 3100. Serial No. 31013780698, SDL Company, England). The total color differences for all non-cleaned and cleaned paper samples were expressed as the color change (ΔE) and measured according to the following Equation [67].

$$\Delta E = \sqrt{(\Delta L)^2 + (\Delta a)^2 + (\Delta b)^2}$$

With a D65 light source and an observed angle of 109°, all of the samples were measured in the visible region, which covers a wavelength range of 400 nm to 700 nm with an interval of 20 nm. The ΔE was expressed using the CIELA B color space's L, a, and b colorimetric coordinates. A cubic form is used to arrange the CIELAB color space. The L axis extends vertically. L can be as large as 100, which stands for white. L has a minimum of zero, which stands for the color black. There are no particular numerical restrictions for the a and b axes. Negative an is green and positive an is red. Negative b is blue, and positive b is yellow. The lower value of ΔE is the closer, the sample is to the standard. ΔE value of 0.00 means the color of the sample is identical to the color of the standard.

Fourier transform infrared spectroscopy (ATR-FTIR)

ATR-FTIR spectrometer (Model 6100, Jasco, Tokyo, Japan) at the National Institute of Standards and Technology (NIST) was used for the ATR-FTIR analysis for the stained and cleaned paper samples [68].

Measurement of mechanical properties

Tensile strength (N) and elongation at break (%) for the stained, cleaned, and aged cleaned paper samples were measured using the testing machine (H5KT, SDL Atlas, Borås, Sweden) at the National Institute for Standards (NIS), at 25 °C and a cross-head speed of 50 mm/min [69].

Statistical analysis

Data on the color changes and mechanical properties (tensile strength and elongation at break) were statistically analyzed with one-way ANOVA. The comparison among means was measured by LSD at a 0.05 level of probability.

Results and discussion

Properties of the prepared stained paper samples

From the 2D, and 3D images of AFM for the stained paper (Figs. 5A, B), it was noticed that the thickness of stain layer on paper was approximately 3.5 µm. From the AFM images (Figs. 6A, B), it was observed that the thickness of low viscosity gel applied over the stained paper was 15 nm. While, the 2D, and 3D images of AFM (Fig. 6C, D) revealed that the thickness of high viscosity gel on the surface of stained paper samples was 18 nm.

Characterization of the prepared nanogels

Characterization of ZnO NPs/Carbopol hybrid nanogel

The data obtained from TEM (Fig. 7A), SEM (Fig. 7B) and AFM (Fig. 7C), images show the spherical shape of ZnO NPs with sharp edges and a particle size of 35 nm. Good desperation in the Carbopol gel without any agglomeration was noticed. The XRD pattern (Fig. 7D) revealed the excellent purity of ZnO NPs/Carbopol hybrid nanogel, where the characteristic ZnO NPs peaks were presented without any secondary products from the synthesis method. However, XRD characteristic peaks of ZnO NPs at 2 Theta = 31.9, 34.6, 36.4, 47.8, 56.9, 63.2, 66.7, 68.34, 69.4, 7 and 77.4°, while Carbopol has zero peaks as measured by XRD as related to its amorphous nature. DLS results (Fig. 5E) showed the size of ZnO NPs/Carbopol hybrid nanogel was 37 nm compatible with TEM results. ZnO NPs/Carbopol hybrid nanogel observed a Zeta potential value of – 33 mV (Fig. 5F), which illustrated its colloidal nature.

Characterization of TiO_2 NPs/Carbopol hybrid nanogel

Characterization of TiO_2 NP/Carbopol hybrid nanogel illustrated in Fig. 8. TEM (Fig. 8A), SEM (Fig. 8B), and 2D and 3D AFM image (Fig. 8C, D) illustrates the spherical shape of TiO_2 NPs with sharp edges and with a size of about 30 nm with good desperation in the Carbopol gel without any agglomeration. XRD results (Fig. 8E) illustrate the excellent purity of TiO_2 NPs/Carbopol hybrid nanogel, where the characteristic peaks of TiO_2 NPs are presented without any secondary products from the synthesis method. However, the peaks of TiO_2 NPs by XRD were characterized at 2 Theta = 27.4°, 36.1°, 41.2° and 54.3°, while Carbopol has zero XRD characteristic peaks due to its amorphous nature. DLS results (Fig. 8F) illustrated that the size of ZnO NPs/Carbopol hybrid nanogel was 34 nm and agreed with TEM results. The zeta potential (Fig. 8G) illustrated the colloidal nature of ZnO NPs/Carbopol hybrid nanogel, in which a value was -39 mV.

Characterization of Fe_3O_4 NPs/Carbopol hybrid nanogel

Characterization of Fe_3O_4 NPs/Carbopol hybrid nanogel is shown in Fig. 9. By XRD measurements (Fig. 9A), the excellent purity of Fe_3O_4 NPs/Carbopol hybrid nanogel was characterized as the peaks of Fe_3O_4 presented without any secondary products at 2 Theta = 30°, 35.4°, 43.03°, 53.4°, 56.91° and 62.5°. Carbopol has no peaks due to its amorphous nature. AFM (Fig. 9B, C) and SEM (Fig. 9D) and TEM (Fig. 9E) images illustrate the sub-spherical shape of Fe_3O_4 with sharp edges and a size of about 35 nm with good desperation and coating of the Carbopol gel without any agglomeration. By DLS (Fig. 9F), the size of Fe_3O_4 NPs/carbopol hybrid nanogel was 55 nm, which compared with TEM results. The Zeta potential (Fig. 9G) of Fe_3O_4 NPs/carbopol hybrid nanogel was − 24 mV, which confirmed its good desperation.

Evaluation of the formulated nanogels in the cleaning process of mud and dust stains

Portable digital microscope (USB microscope)

The images of a digital microscope play an important role in evaluating the surface damage of the object [70]. The image obtained from the USB microscope for the paper sample before the treatment with the prepared nanogels (Fig. 10) referred that the surface of the untreated sample is full of spots and impurities. In the untreated sample, the surface of the paper was covered with impurities and mud stains.

Figure 11 shows the treatment with TiO_2NPs/carbopol hybrid nanogel before and after aging. The mud stains and impurities still existed, when the samples were cleaned with TiO_2 NPs/carbopol hybrid low

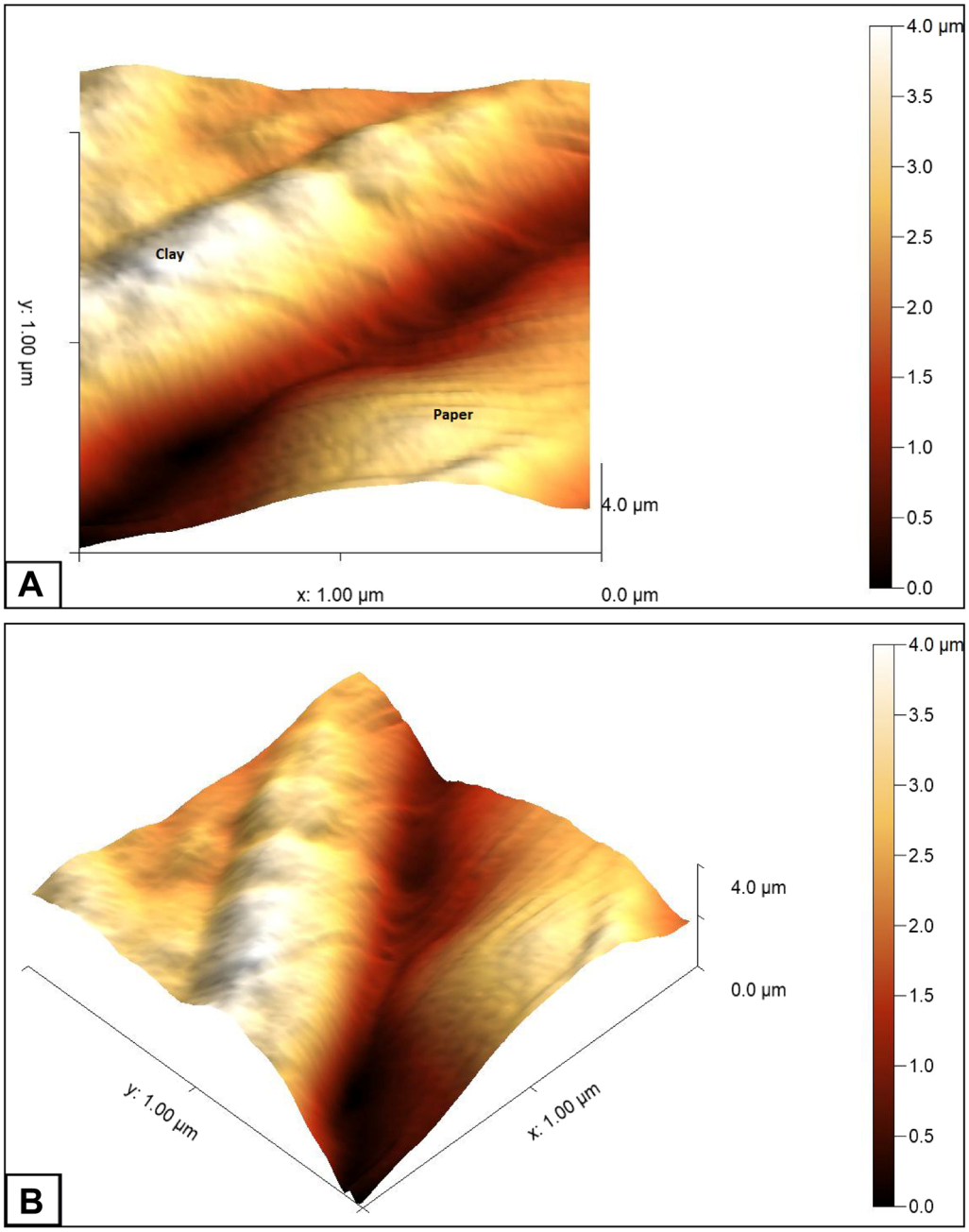

Fig. 5 AFM images of the stained paper; **A** 2D image; **B** 3D image

viscosity (LV) nanogel (Fig. 11A, B), which indicated the inefficiency of this nanogel. After the treatment with TiO_2 NPs/carbopol hybrid high viscosity (HV) nanogel (Fig. 11C, D), the presence of mud stains and impurities were observed, with the absence of the fibers, which significantly indicated the inefficiency cleaning process, when using this gel.

After using ZnO NPs/Carbopol hybrid LV nanogel (Fig. 12A, B), the appearance of the white surface of the paper was found with a slight residue of mud stain, which evidence the efficiency of this gel. After using ZnO NPs/Carbopol hybrid HV nanogel (Fig. 12C, D), the paper fibers were clearly observed with a white surface and a slight trace of a mud stain was stained.

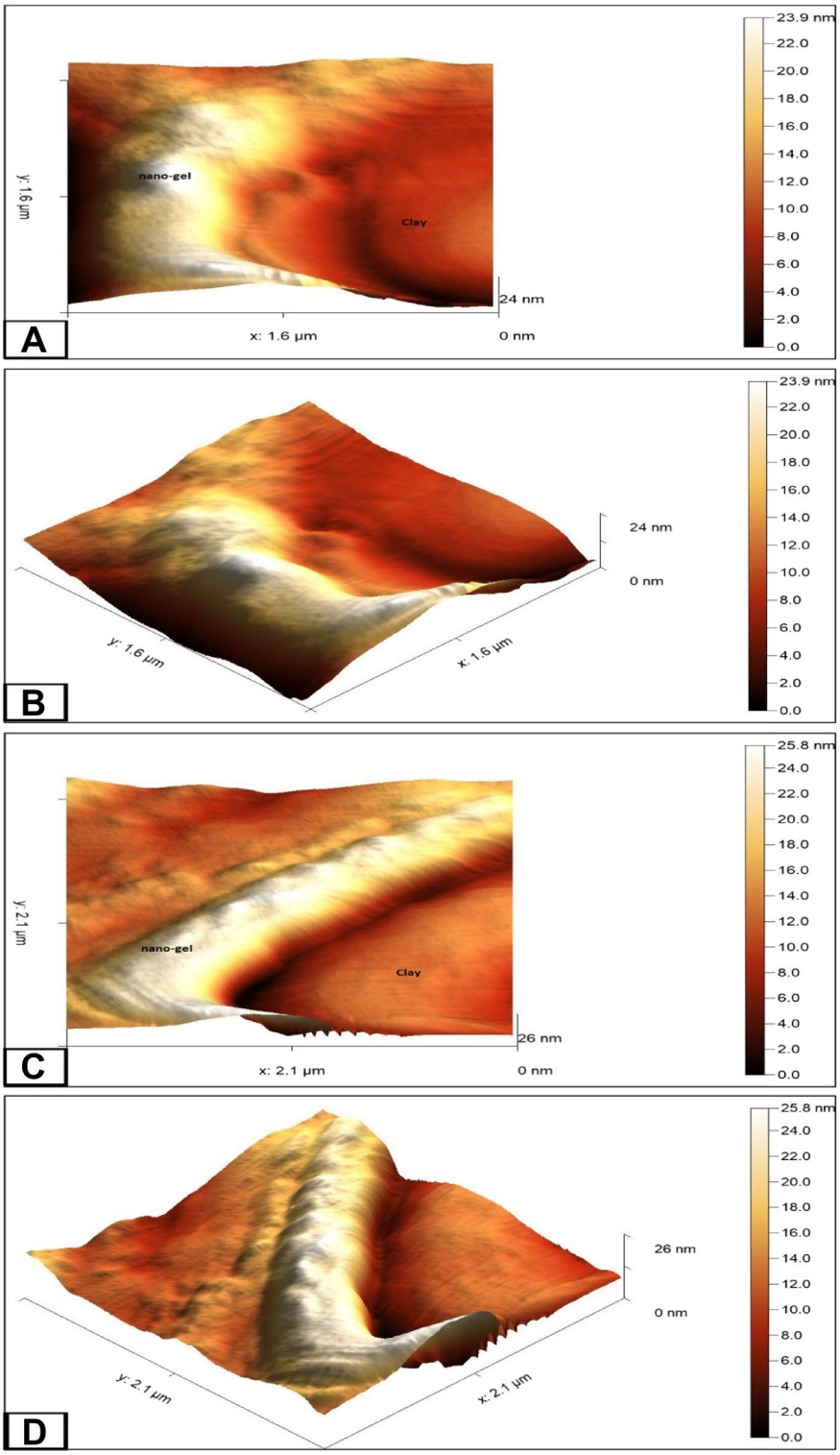

Fig. 6 AFM images of applied nanogel over paper; **A**, **B** 2D, and 3D of low viscosity gel; **C**, **D** 2D, and 3D of high viscosity gel

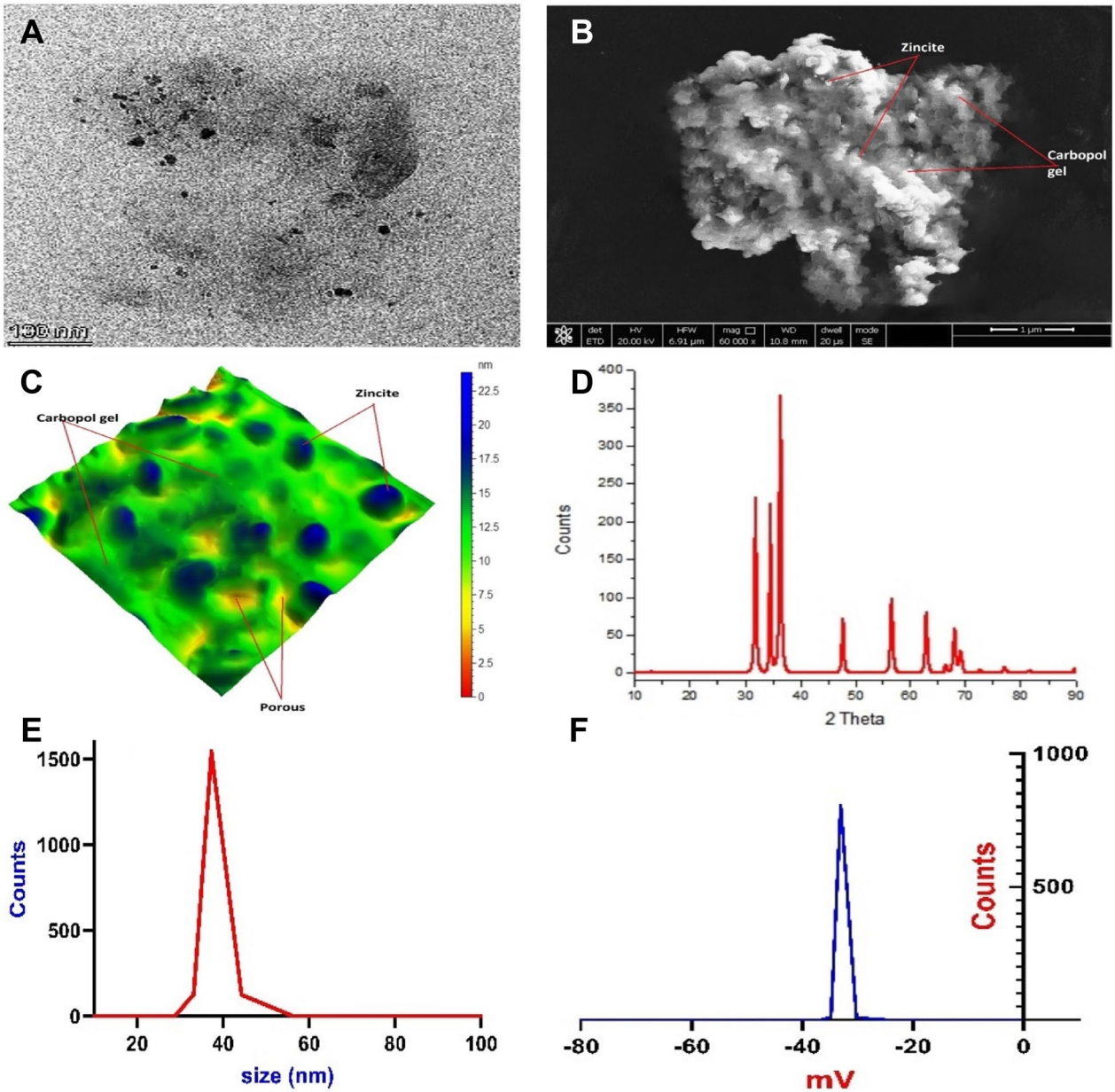

Fig. 7 The characterization of ZnO NP/Carbopol hybrid nanogel; **A** TEM; **B** SEM; **C** 3D AFM image; **D** XRD; **E** DLS and **F** Zeta potential

The fibers did not appear clearly and there was a lot of mud remaining when the sample was treated with Fe_3O_4 NPs/carbopol LV hybrid nanogel (Fig. 13A, B), which indicated the inefficiency of this nanogel. After the treatment with the Fe_3O_4 NPs/carbopol HV hybrid nanogel (Fig. 13C, D), the surface of the paper appeared to be white with a slight residue of stains, which supported the efficiency of this nanogel.

From the above results, the effect of ZnO NPs/Carbopol hybrid HV nanogel was the best, where the surfaces of the cleaned paper appeared to be white. Additionally, there were no substances fully treated. In every treatment, there was a residue of impurities and traces of a mud stain.

Nanogels have been used widely; for example, a gel of ZnO NPs modified with hydroxyethyl cellulose has demonstrated its efficacy in simulating the healing of skin wounds by primary tension and has a strong regenerative effect on burn wounds [39]. SiO_2-TiO_2-ZrO_2 nanocomposites with a content of TiO_2 between 8% and 9.5% and ZrO_2 between 0.5% and 2% exhibit complete insolubility in a highly alkaline medium, enable the formation

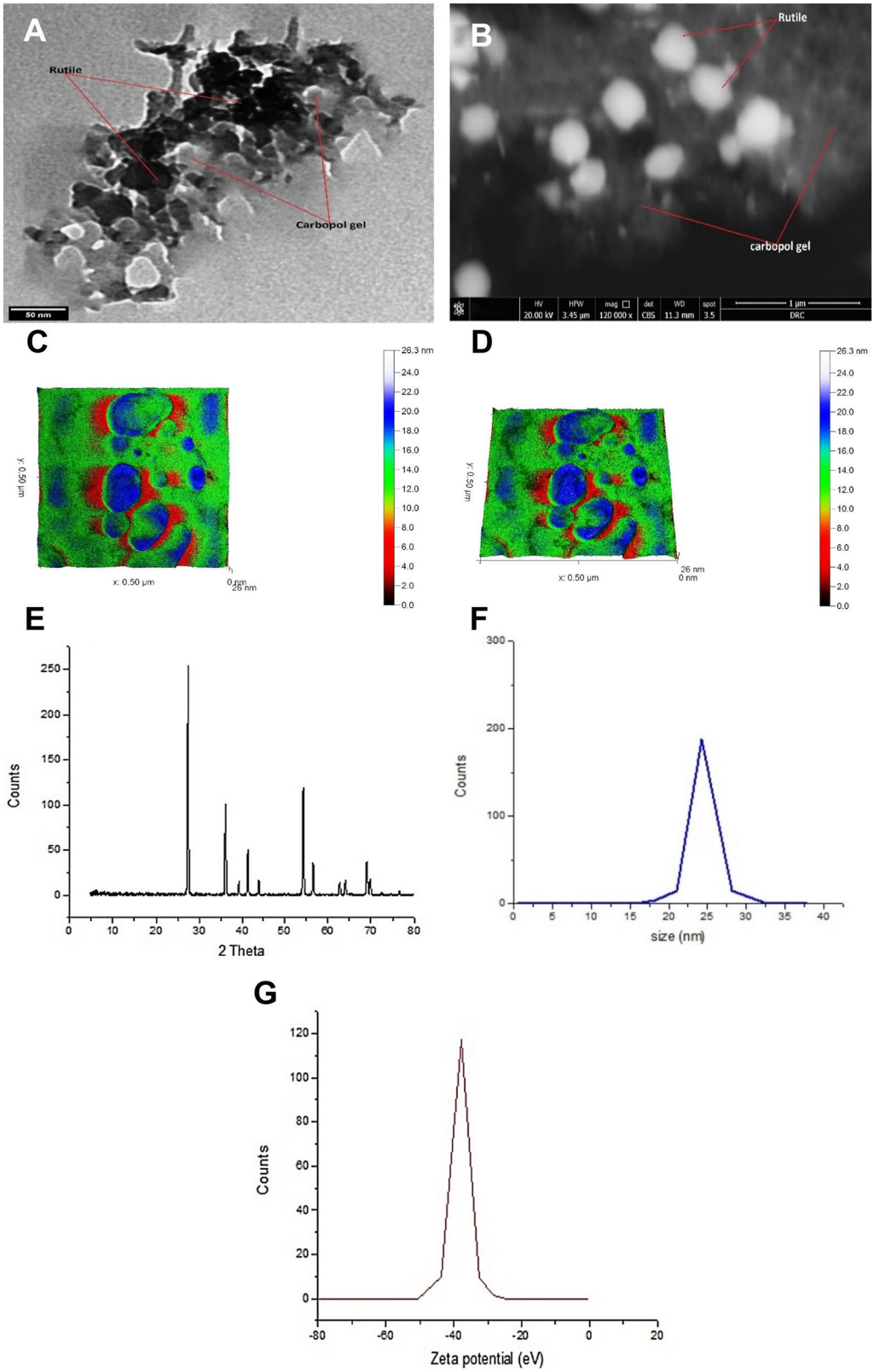

Fig. 8 Characterization of TiO_2 NP/Carbopol hybrid nanogel; **A** TEM; **B** SEM; **C**, **D** AFM; **E** XRD; **F** DLS; **G** Zeta potential

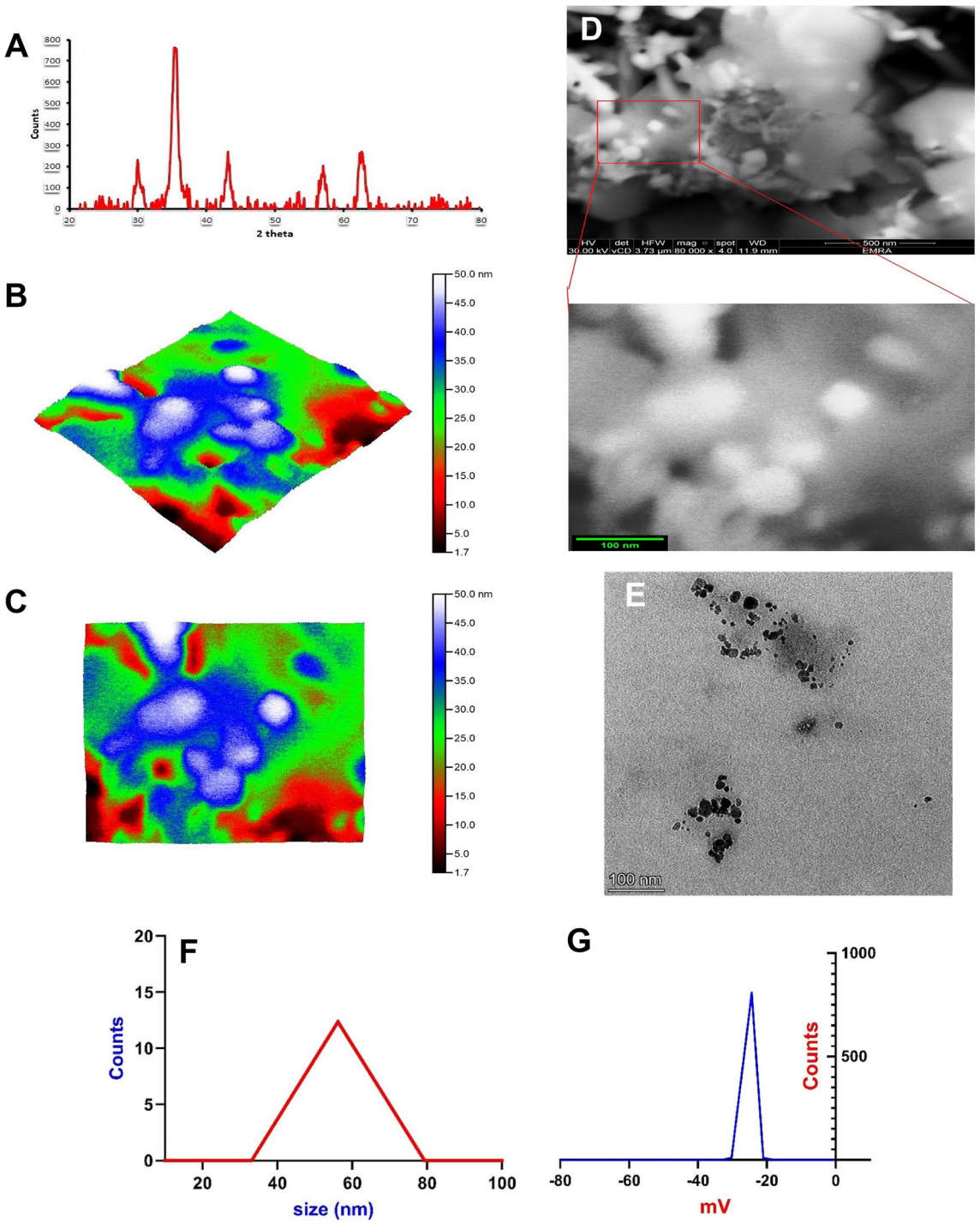

Fig. 9 Characterization of Fe_3O_4 NP/carbopol hybrid nanogel; **A** XRD; **B**, **C** AFM; **D** SEM; **E** TEM; **F** DLS; **G** Zeta potential

of uniform structure on paint and varnish coatings, and shield the car surface from UV radiation [49].

Attractive Fe_3O_4 NPs have been developed as emerging materials for its broad scope use in various fields [71]. In the pre-concentration and immobilization of 2,4,4′-trichlorobiphenyl from vast volumes of aqueous solutions in the cleanup of polychlorinated biphenyl pollution, Fe_3O_4 NPs grafted graphene oxide (Fe_3O_4@GO) was an appropriate material [72]. Fe_3O_4 NPs showed no toxicity in water cleaning operations and might be

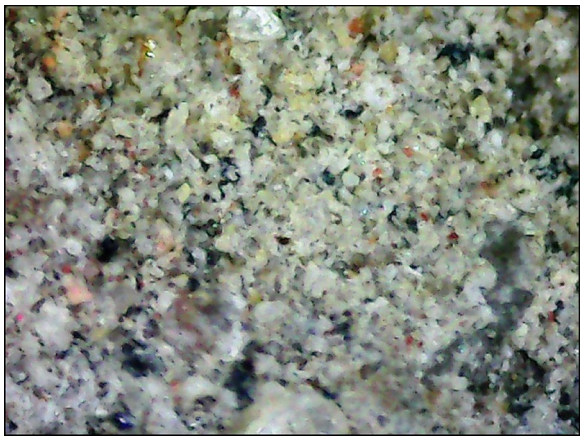

Fig. 10 Digital microscope image of stained sample before cleaning

employed as absorbents for Pb (II) removal [73]. When methylene blue dye was exposed to green LED light and Fe_3O_4/ZnO-modified natural pumice, a high degradation yield was seen [74]. Another investigation into thrombolytic ratio testing has shown that employing magnetically controlled urokinase-coated Fe_3O_4 NPs rather than a pure urokinase solution considerably increases the efficiency of thrombus cleaning [75]. Fe3O4@UiO-66-NH2/PVDF-co-CTFE mixed matrix membrane showed excellent anti-fouling performance for wastewater treatment in complex environments [76].

Surface morphology by scanning electron microscope

The SEM image (Fig. 14) of the untreated paper samples before treatment with different nanogels showed the presence of a thick layer of mud and dust satins, which led to the hide of the paper's fibers [1]. Additionally, it was clear from the microscopic images that the accelerated thermal aging impacted the structure of the untreated samples, where apparent destruction of untreated paper fibers was observed. Furthermore, the roughness of the fibers and the tearing deformation of paper fibers were also noticed.

The SEM images of the treated paper sample with TiO_2 NPs/carbopol hybrid LV nanogel (Fig. 15A, B) and HV nanogel (Fig. 15C, D) gave good results compared to the untreated sample, but the surface still covered with the dust layer and consequently the disappearance of paper's fibers. This result referred to the low efficiency of these treatments.

The SEM images of the treated paper samples with ZnO NPs/carbopol hybrid LV nanogel (Fig. 16A, B)

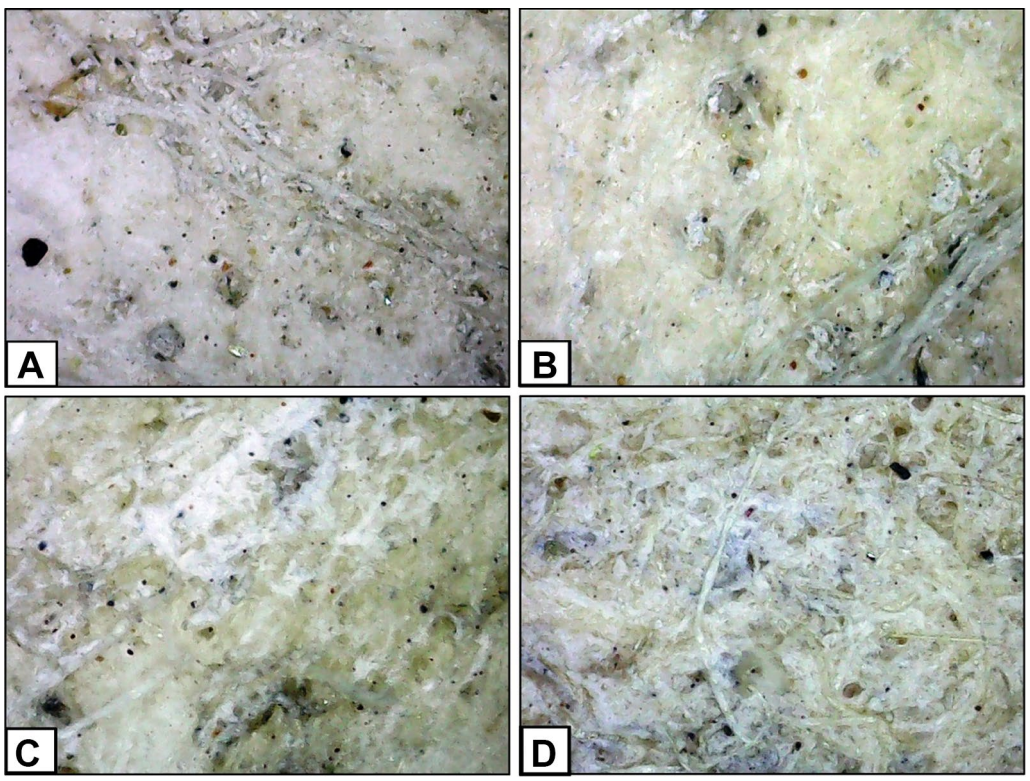

Fig. 11 Digital microscope images of cleaned paper samples with TiO_2 NP/carbopol hybrid nanogel before and after aging; **A** Cleaned sample with LV nanogel; **B** Aged cleaned sample with LV nanogel; **C** Cleaned sample with HV nanogel; **D** Aged cleaned sample with HV naogel

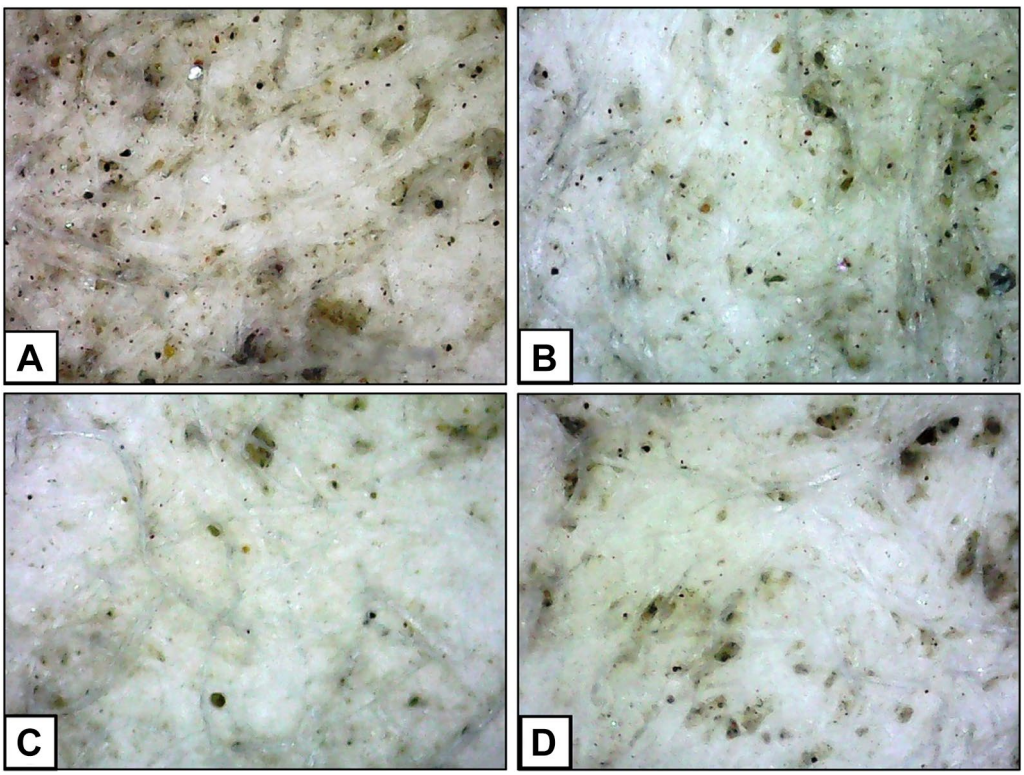

Fig. 12 Digital microscope images of cleaned paper samples with ZnO NP/carbopol hybrid nanogel before and after aging; **A** Cleaned sample with LV nanogel; **B** Aged cleaned sample with LV nanogel; **C** Cleaned sample with HV nanogel; **D** Aged cleaned sample with HV nanogel

gave good results compared to the untreated sample, where the simple presence of paper sample was. Interestingly, the treated sample with ZnO NPs/carbopol hybrid HV nanogel (Fig. 16C, D, E) gave the best results, especially in the presence of paper fibers.

The SEM images of the treated samples with Fe_3O_4 NPs/carbopol hybrid nanogel revealed (Fig. 17) that the HV nonogel gave the best results compared to the treated sample with LV nanogel. The treated sample with LV nanogel showed little difference compared to the untreated sample.

From the previous results, it was worth noting that the amount of residue was high at a treated with ZnO NPs/carbopol hybrid nanogel (after aging), Fe_3O_4 NPs/carbopol hybrid nanogel (after aging), both high-treated paper's surface with Fe_3O_4 NPs/carbopol hybrid HV nanogel and TiO_2 NPs/carbopol hybrid HV nanogel results on the processed paper after aging. Both treated paper's surface with TiO_2 NPs/carbopol hybrid HV nanogel after aging, ZnO NPs/carbopol hybrid HV nanogel after aging, and ZnO NPs/carbopol hybrid LV nanogel before aging are good results, but not as efficient as the previous materials.

Measurements of color change by spectrophotometer

Comparing the results of the color change (ΔE) values for the samples before and after treatment (Table 1), it was noticed that a significant ΔE occurred in the treated sample with ZnO NPs/Carbopol hybrid HV nanogel, for which the ΔE value was relatively high compared to others treatment with different nanogels, especially Fe_3O_4 NPs/carbopol hybrid LV nanogel, as it gave the worst results in cleaning treatment, where it recorded 5.13.

The results of the table confirmed that after the artificial aging, the values of ΔE in all treated samples decreased significantly, where ΔE of the treated sample with ZnO NPs/Carbopol hybrid nanogel at the HV recorded at 19.32 which is considered the highest value. On the other hand, the aged treated sample with Fe_3O_4 NPs/carbopol hybrid nanogel at LV recorded the lowest ΔE value of 2.00.

The apparent improvement in the values of ΔE can be attributed to two reasons; (1) the role of the heat during the aging in dryness of the residues; (2) nanogel can react as a bleaching agent, which can improve the color change after again the result of bleaching [77].

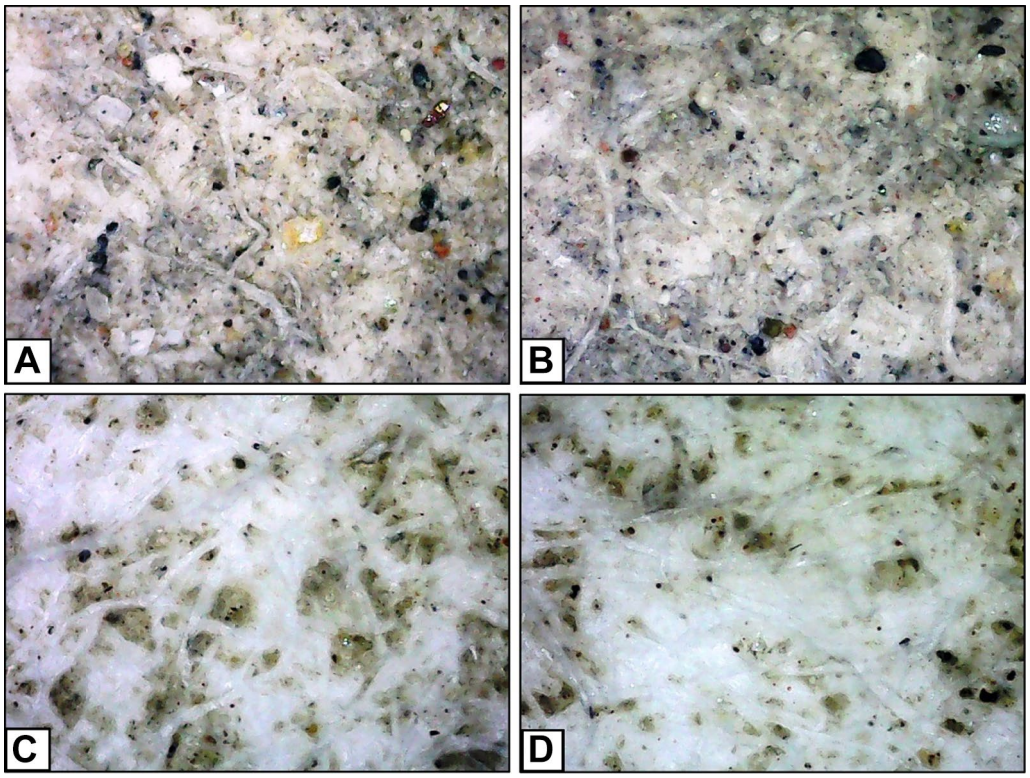

Fig. 13 Digital microscope images of cleaned paper samples with Fe_3O_4 NP/carbopol hybrid nanogel before and after aging; **A** Cleaned sample with LV nanogel; **B** Aged cleaned sample with LV nanogel; **C** Cleaned sample with HV nanogel; **D** Aged cleaned sample with HV nanogel

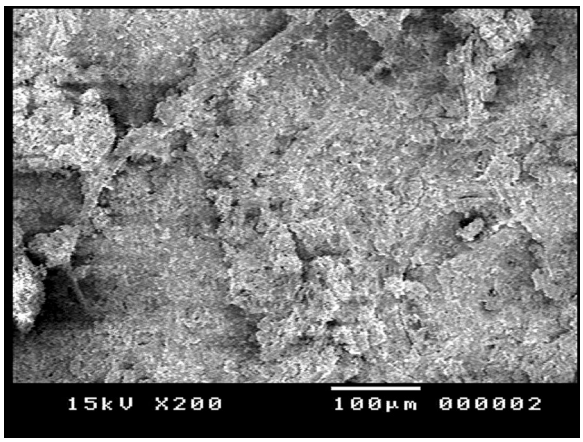

Fig.14 SEM image of stained paper sample before cleaning

There was also a clear difference between the values of the ΔE according to the type of nanogels used after the accelerating aging, where ΔE of the aged treated samples with ZnO NPs/carbopol hybrid nanogel and Fe_3O NPs/carbopol hybrid nanogel recorded values of 19.32 and 15.76, respectively, which confirmed that the ZnO NPs/carbopol hybrid nanogel had a pivotal role in increasing the values of ΔE, which referred to the efficiency of this gel in removing the dust stains. Comparing these results after aging, it was observed that the lowest ΔE (2.00) was found in the sample treated with the LV of Fe_3O_4 NPs/carbopol hybrid nanogel. This was followed by the treated sample with the LV of TiO_2 NPs/carbopol hybrid nanogel (ΔE 9.11), the treated sample with the HV of TiO_2 NPs/carbopol hybrid nanogel (ΔE 13.88) and the use of ZnO NPs/carbopol hybrid LV nanogel (ΔE 15.13).

Measurements of mechanical properties

The data obtained in Table 2 show that the treated sample with ZnO NPs/carbopol hybrid nanogel at HV gave the highest tensile strength (56.40 N). This result revealed that a good cleaning treatment was obtained compared to other treatments. Followed by a treated sample with Fe_3O_4 NPs/carbopol hybrid HV nanogel (53.8 N), then a treated sample with LV form of ZnO NPs/carbopol hybrid nanogel (37.59 N). On the other hand, the treated sample with Fe_3O_4 NPs/carbopol hybrid nanogel at LV form gave the worst value (18.93 N).

The results of tensile strength for the aged treated samples (Table 2) showed that the aged treated sample with HV form of ZnO NPs/carbopol hybrid nanogel gave the highest tensile strength value of 56.0 N, compared to the

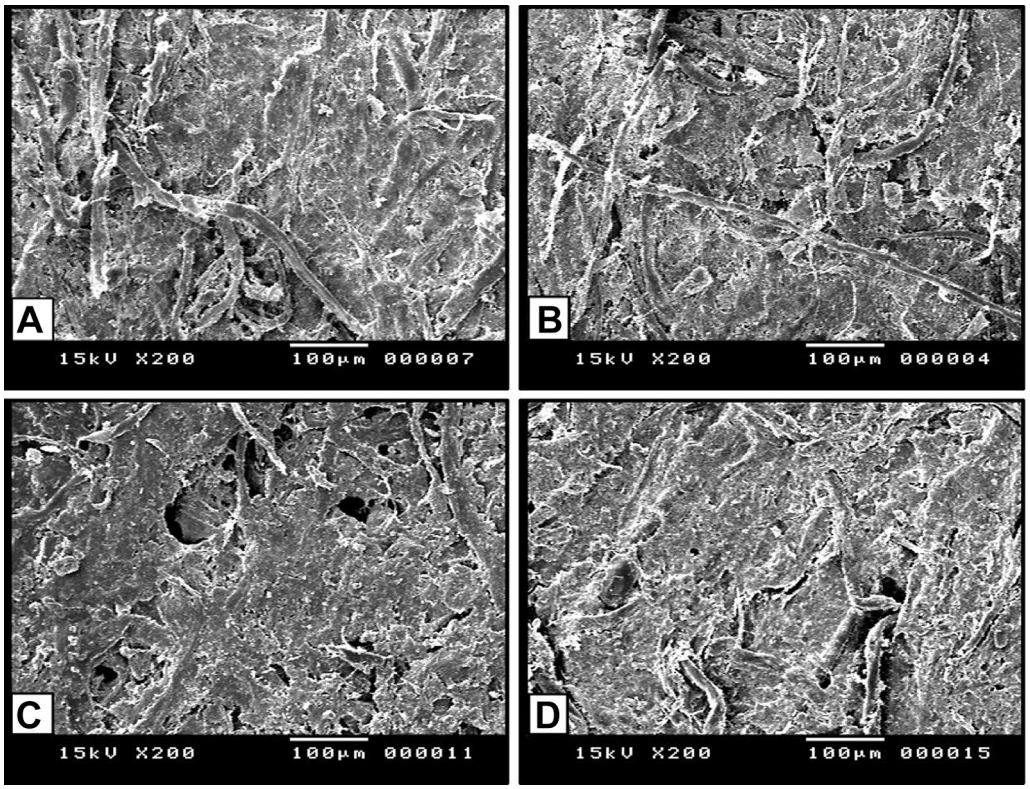

Fig. 15 SEM images of cleaned paper samples with TiO_2 NP/carbopol hybrid nanogel before and after aging; **A** Cleaned sample with LV nanogel; **B** Aged cleaned sample with LV nanogel; **C** Cleaned sample with HV nanogel; **D** Aged cleaned sample with HV nanogel

untreated and treated paper samples with other treatments. Additionally, little difference was observed with the treated sample before aging, which referred to the efficiency of this treatment against thermal aging. In contrast, the aged treated sample with LV form of Fe_3O_4 NPs/carbopol hybrid nanogel gave the lowest value (17.35 N).

The data obtained in Table 2 showed that the untreated paper sample has the lowest elongation value (0.568%), which may be due to the effect of dust remains and accelerated thermal aging. The treated samples with the HV form of ZnO NPs/carbopol hybrid nanogel gave the highest value of elongation (1.398%), followed by the HV form of Fe_3O_4 NPs/carbopol hybrid nanogel (1.239%), LV form of ZnO NPs/carbopol hybrid nanogel (1.159%), TiO_2 NPs/carbopol hybrid HV nanogel (1.013%), TiO_2 NPs/carbopol hybrid LV nanogel (0.920%) and finally, the treated samples with Fe_3O_4 NPs/carbopol hybrid LV nanogel, which own the lowest value (0.815%).

The results of elongation at break values for all treated samples with different nanogels revealed an improvement in the elongation values compared to the uncleaned sample. By comparing the values of the elongation at break for the cleaned paper samples after accelerated thermal aging (Table 2), it was noticed that the treated paper sample with ZnO NPs/carbopol hybrid HV nanogel gave the highest value (1.328%). This result referred to the high resistance of this treatment against thermal aging. In contrast, the aged treated sample with Fe_3O_4 NPs/carbopol hybrid LV nanogel gave the lowest value (17.35%).

From the previous results, it concluded that the treated sample with ZnO NPs/carbopol hybrid HV nanogel gave the best mechanical properties (tensile strength and elongation at break) either before or after thermal aging. This referred to the removal of the accumulated dust and an increase in the mechanical properties of the treated paper. On the other hand, the treated sample with Fe_3O_4 NPs/carbopol hybrid LV nanogel gave the lowest value, which referred to the non-efficiency of this treatment for cleaning the stains from the paper samples.

The performance properties of the nano-gel are also impacted by variations in the nanoparticle concentration content. Properties including viscosity, swelling capacity, and cleaning behavior can alter as the amount of nanoparticles in a material rises. Depending on how the nano-gel is being used specifically, these alterations can be beneficial or detrimental. As a result, to optimize the nano-gel's performance characteristics for a particular

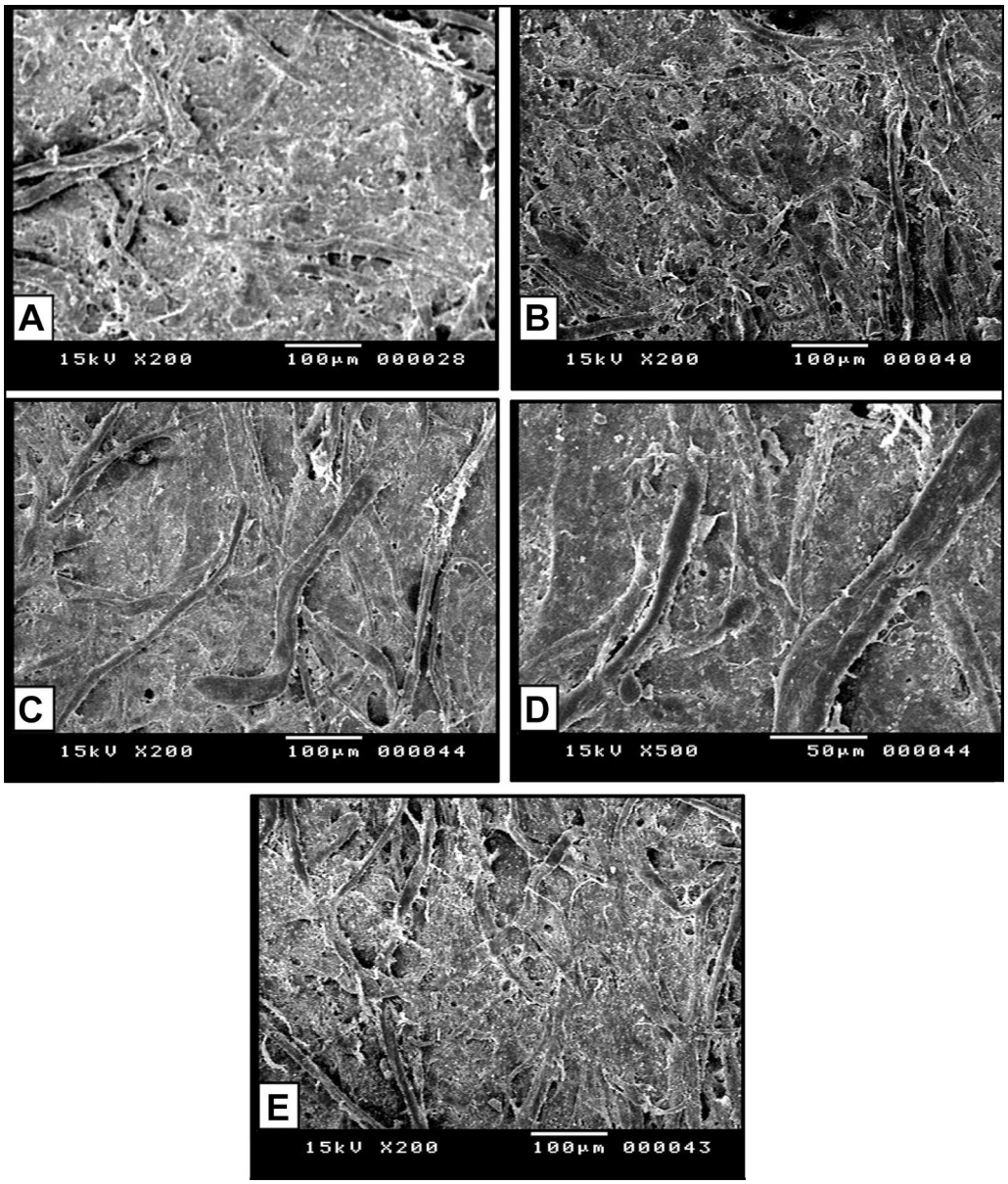

Fig.16 SEM images of cleaned paper samples with ZnO NP/carbopol hybrid nanogel before and after aging; **A** Cleaned sample with LV nanogel; **B** Aged cleaned sample with LV nanogel; **C**, **D** Cleaned sample with HV nanogel; **E** Aged cleaned sample with HV nanogel

application, careful control of the nanoparticle content is required.

Fourier transform infrared spectroscopy

From the data obtained for the aged untreated paper samples (Fig. 18), it was noticed the disappearance of the characteristic peaks of cellulose (Table 3), which referred to decompose of paper under the influence of accelerated industrial aging and the covering of the paper surface with a thick mud stain. Consequently, the characteristic peaks of mud and soil remain such as O–H (3698 cm^{-1}), O–H (3500 cm^{-1}), C–H (2900 cm^{-1}), C=O, C=C (1600 cm^{-1}), C–H (1395 cm^{-1}), C–O–C (1163 cm^{-1}), and O–H (666 cm^{-1}) were observed [78]. The ATR-FTIR spectra of the aged untreated samples (Fig. 18) observed the functional groups of OH at 3698 cm^{-1} and 3500 cm^{-1}, and CH_2 at 2850 cm^{-1}. Additionally, the characteristic functional groups of cellulose were not observed, which is considered to be an indication of the disappearance of cellulose under the mud layer.

Furthermore, methyl and methylene groups can be detected at 2918 and 2850 cm^{-1} [79], the hydroxyl group

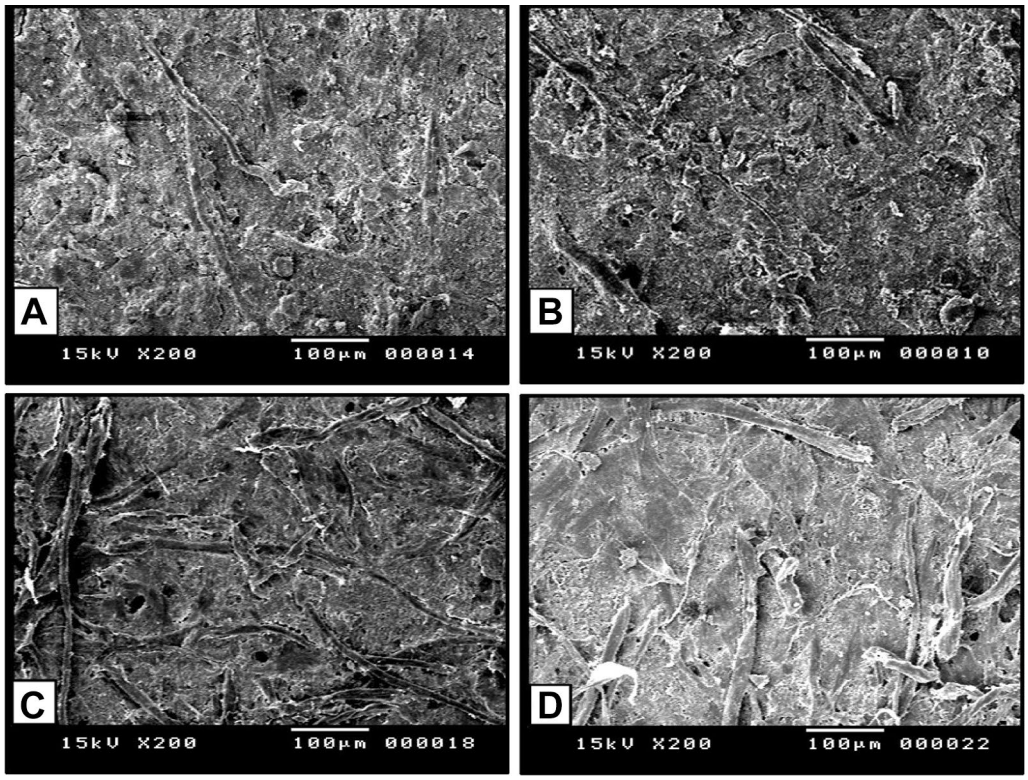

Fig. 17 SEM images of cleaned paper samples with Fe_3O_4 NP/carbopol hybrid nanogel before and after aging; **A** Cleaned sample with LV gel; **B** Aged cleaned sample with LV nanogel; **C** Cleaned sample with HV nanogel; **D** Aged cleaned sample with HV nanogel

Table 1 The results of color change for the aged mud stained paper, treated and aged treated paper samples

Samples	*L*	*a*	*b*	ΔE	*L*	*a*	*b*	ΔE
Aged stained sample before treatment	63.47	1.75	9.39	0.0G	63.47	1.75	9.39	0.0G
TiO_2 NP/carbopol hybrid nanogel								
Low viscosity gel					High viscosity gel			
Treated sample before ageing	73.78	2.63	13.20	11.03C ± 0.015	77.42	2.25	12.40	14.28E ± 0.026
Treated sample after ageing	70.57	3.90	14.67	9.11D ± 0.010	76.83	2.36	13.10	13.88F ± 0.010
ZnO NP/carbopol hybrid nanogel								
Low viscosity gel					High viscosity gel			
Treated sample before ageing	79.00	1.90	11.05	15.62A ± 0.010	83.04	1.53	12.11	19.76A ± 0.010
Treated sample after ageing	78.27	2.22	12.52	15.12B ± 0.021	82.61	1.64	12.03	19.32B ± 0.010
Fe_3O_4 NP/carbopol hybrid nanogel								
Low viscosity gel					High viscosity gel			
Treated sample before ageing	67.84	2.77	11.87	5.13E ± 0.011	80.88	1.33	10.28	17.44C ± 0.011
Treated sample after ageing	65.06	2.35	10.44	2.003F ± 0.011	79.21	1.07	9.86	15.76D ± 0.017
LSD 0.05				0.0223				0.0251

Means with the same letter within the same column are not significantly different according to LSD at 0.05 level of probability

at 3296 and 3620 cm^{-1} [79, 80], carboxyl at 1030 cm^{-1}, hydroxyl at 3319 cm^{-1}, cellulose at 3660–2800 and 1650–400 cm^{-1}, CH, -OH and C–O at 1420–1430 cm^{-1}, CO_3 and $CaCO_3$ at 1475 cm^{-1}, and the natural hydrous silicates at 1620–1642 cm^{-1} [1, 81].

From the ATR-FTIR spectra of the treated sample with TiO_2 NPs/carbopol hybrid nanogel at LV before aging (Fig. 18), the appearance of CH (2870 cm^{-1}) and C–O–C (982 cm^{-1}) is related to cellulose and many functional groups of mud. Additionally, the

Table 2 The results of mechanical properties (Tensile strength and Elongation at break) for the aged dust-stained paper, treated paper, and aged treated paper samples

Samples	Tensile strength (N)	Elongation at break (%)	Tensile strength (N)	Elongation at break (%)
Aged stained sample before treatment	17.21G ± 0.010	0.568G ± 0.002	17.21G ± 0.010	0.568G ± 0.002
TiO_2 NP/carbopol hybrid nanogel				
Low viscosity nanogel			High viscosity nanogel	
Treated sample before aging	30.05C ± 0.010	0.920C ± 0.001	36.60E ± 0.010	1.013E ± 0.0011
Treated sample after aging	26.88D ± 0.0115	0.904D ± 0.001	35.28F ± 0.015	0.976F ± 0.0015
ZnO NP/carbopol hybrid nanogel				
Low viscosity naogel			High viscosity nanogel	
Treated sample before aging	37.58A ± 0.011	1.159A ± 0.002	56.40A ± 0.010	1.398A ± 0.001
Treated sample after aging	37.08B ± 0.010	1.049B ± 0.001	56.0B ± 0.010	1.328B ± 0.001
Fe_3O_4 NP/carbopol hybrid nanogel				
Low viscosity nanogel			High viscosity nanogel	
Treated sample before aging	18.93E ± 0.011	0.815E ± 0.001	53.8C ± 0.010	1.239C ± 0.001
Treated sample after aging	17.35F ± 0.0115	0.654F ± 0.001	42.10D ± 0.010	1.200D ± 0.001
LSD 0.05	0.0191	0.0026	0.0191	0.0023

Means with the same letter within the same column are not significantly different according to LSD at 0.05 level of probability

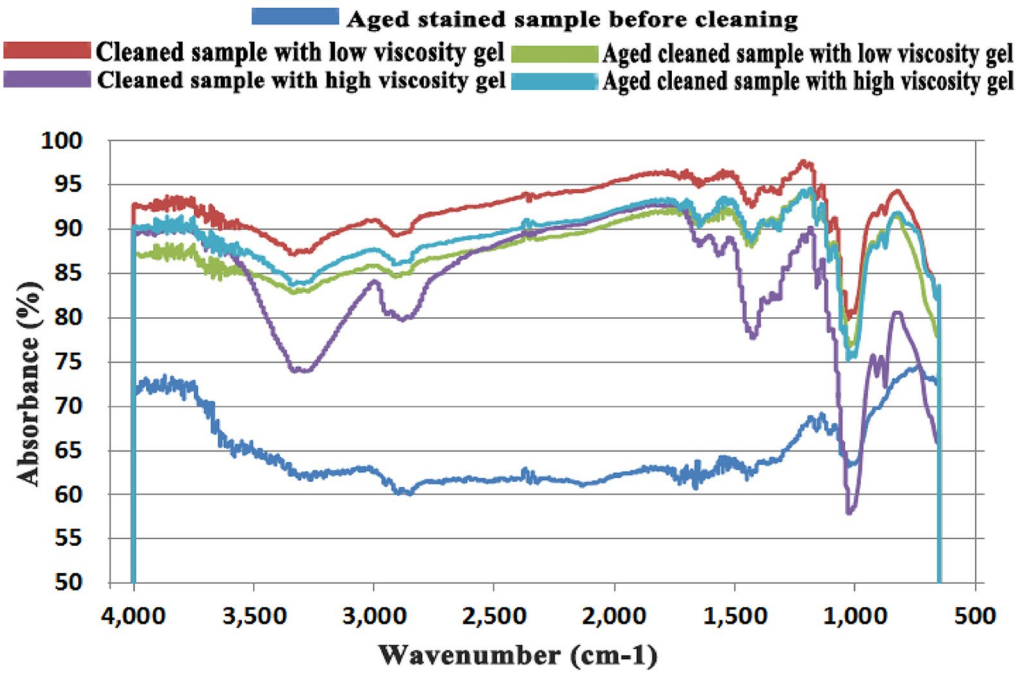

Fig. 18 FTIR of aged untreated and treated paper samples with TiO_2 NP/carbopol hybrid nanogel

disappearance of the most characteristic functional groups of cellulose referred to the presence of mud stains and the low efficiency of the tested TiO_2 NPs/carbopol hybrid LV nanogel in removing mud dust. This result confirmed the data obtained from the digital and SEM microscopes, where their micrographs revealed the presence of mud stains on the treated paper surface and the disappearance of paper fibers in different places of the examined paper. From the ATR-FTIR spectra of the treated sample with TiO_2 NPs/carbopol hybrid LV nanogel after aging (Fig. 18), it was noticed the disappearance of most functional groups, which referred to the effect of accelerated thermal aging on this treated sample.

Table 3 The characteristic function groups were identified in the treated and aged treated paper samples with TiO2NP or ZnONP, and Fe3O4NP/ carbobol nanogel

Characteristic peaks of cellulose	TiO_2 NP/carbobol nanogel				ZnO NP/carbopol hybrid nanogel				Fe_3O_4 NP/carbobol nanogel			
	Low viscosity		High viscosity		Low viscosity		High viscosity		Low viscosity		High viscosity	
	Before ageing	After ageing	Before ageing	After ageing	Before ageing	After ageing	Before ageing	After ageing	Before ageing	After ageing	Before ageing	After ageing
OH	–	–	3290	–	–	–	3330	3330	–	–	3230	3260
Intensity (%)	–	–	73.90	–	–	–	93.80	84.20	–	–	85.09	83.90
CH	2870	–	–	–	2880	2890	2910	2910	–	–	2856	2849
Intensity	89.60	–	–	–	89.70	89.50	96.00	85.90	–	–	87.80	86.84
C = O, C = C	–	–	–	–	1600	–	1640	1640	–	1677	1605	–
Intensity (%)	–	–	–	–	95.00	–	99.20	90.50	–	87.26	92.37	–
CH	–	–	1400	–	1400	1410	1420	1360	1419	1409	–	–
Intensity (%)	–	–	78.40	–	93.90	93.30	97.80	89.70	90.10	85.26	–	–
C–O–C	982	982	966	989	–	–	1030	1030	974	991	998	992
Intensity (%)	81.30	78.00	58.80	75.80	–	–	84.50	79.70	84.51	76.92	81.49	77.85
O–H	–	777	–	666	650	787	809	672	–	–	–	–
Intensity (%)	–	90.90	–	83.70	84.50	93.90	96.00	85.10	–	–	–	–

(–) Means that the function group not observed

From the ATR-FTIR spectra of the treated sample with TiO_2 NPs/carbopol hybrid HV nanogel before aging (Fig. 18) it was noticed some characteristic functional groups of cellulose such as OH (3290 cm^{-1}), CH (1400 cm^{-1}) and C–O–C (1163 cm^{-1}). Additionally, the disappearance of some other functional groups referred to the presence of mud stains on the surface. By comparing the treated samples with TiO_2 NPs/carbopol hybrid nanogels, it was observed that the treated sample with HV nanogel was more effective than the treated sample with the LV nanogel. The ATR-FTIR spectra of the treated sample with LV nanogel after aging (Fig. 18) revealed the effect of thermal aging on the treated paper, where the disappearance of most functional groups found before aging, where C–O–C found at 989 cm^{-1} and O–H at 666 cm^{-1}.

The treated paper samples with ZnO NPs/carbopol hybrid LV nanogel before aging (Fig. 19) showed the presence of the functional groups of cellulose CH (2880 cm^{-1}), C=O (1600 cm^{-1}), CH (1400 cm^{-1}) and OH (650 cm^{-1}) related to cellulose and the disappearance of OH and C–O–C groups referred to the presence of some traces from mud stains. The ATR-FTIR spectra of the treated samples after aging showed the presence of the characteristic peaks noticed before aging, but with shifting in the position of functional groups, where CH at 2890 cm^{-1}, CH at 1410 cm^{-1} and OH at 787 cm^{-1}. Additionally, it was noticed the disappearance of the functional group C=O. The shifting in position of most functional groups and the disappearance of some other groups may be due to the effect of the accelerated thermal aging process.

From the ATR-FTIR spectra of the treated sample with ZnO NPs/carbopol hybrid HV nanogel (Fig. 19) it was characterized the functional groups of cellulose OH (3330 cm^{-1}), CH (2910 cm^{-1}), C=O (1640 cm^{1}), CH (1420 cm^{-1}), C–O–C (1030 cm^{-1}) and OH (809 cm^{-1}), with almost the disappearance of characteristic peaks of mud. The ATR-FTIR spectra of the treated sample after aging with ZnO NPs/carbopol hybrid HV nanogel showed the characteristic functional groups of cellulose OH (3330 cm^{-1}), CH (2910 cm^{-1}), C=O (1640 cm^{-1}), CH (1360 cm^{-1}), C–O–C (1030 cm^{-1}), and OH (672 cm^{-1}) at almost the same positions of the treated sample before aging. Additionally, it was not observed new functional groups, which referred to the resistance of the treated sample against the thermal aging process.

By comparing the ATR-FTIR spectra of the treated samples with ZnO NPs/carbopol hybrid nanogel at different concentrations and the untreated sample, it was noticed the efficiency of the ZnO NPs/carbopol hybrid nanogel in the cleaning process, but the HV form gave the best results.

The treated paper samples with Fe_3O_4 NP/carbopol hybrid LV nanogel before aging (Fig. 20) observed the disappearance of most characteristic functional groups of cellulose and the presence of the characteristic peaks of mud. The occurrence of the CH group at 1419 cm^{-1}

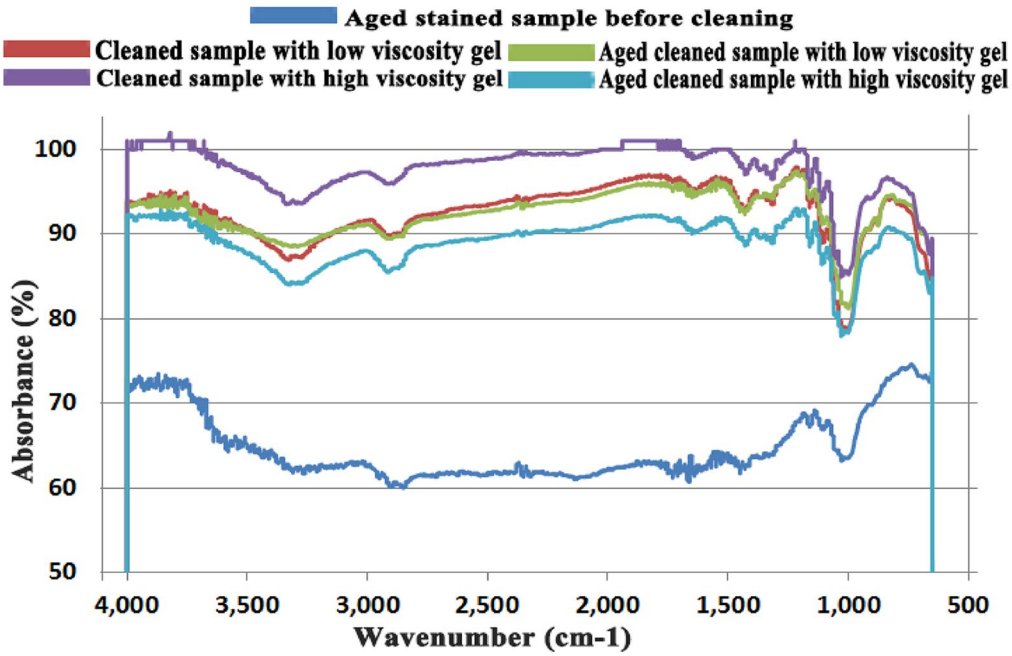

Fig. 19 FTIR of aged untreated and treated paper samples with ZnO NP/carbopol hybrid nanogel

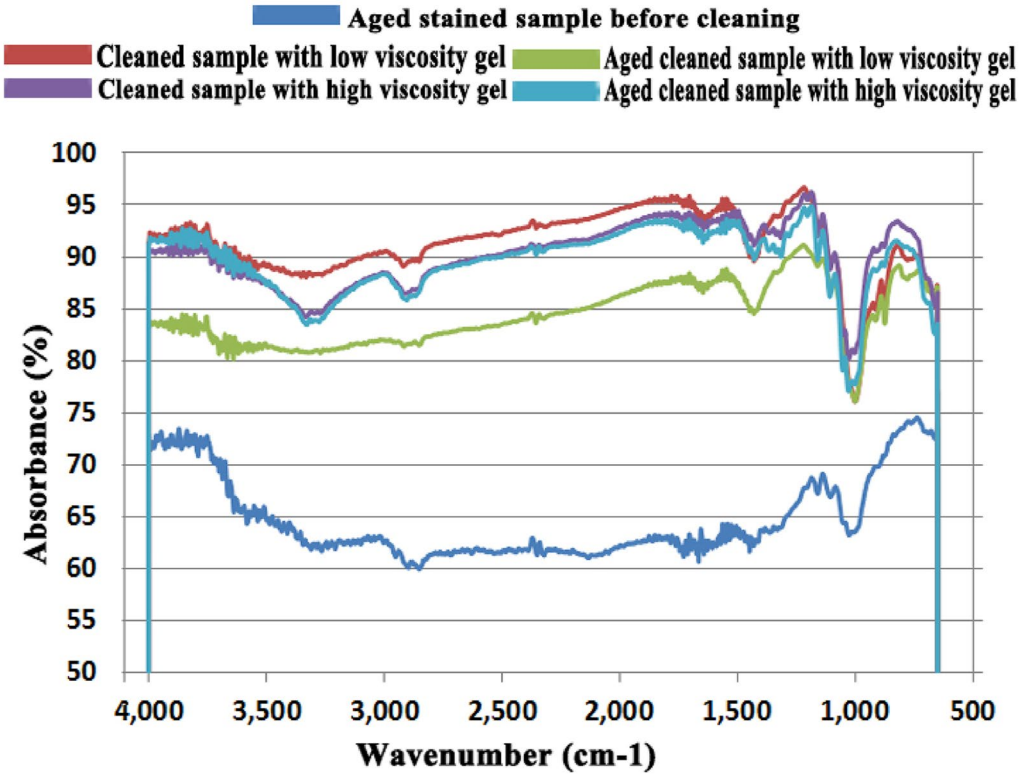

Fig. 20 FTIR of aged untreated and treated paper samples with Fe_3O_4 NP/carbopol hybrid nanogel

and C–O–C at 974 cm^{-1}, referred to the presence of mud stain, which led to the inefficiency of the tested nanogel in the cleaning process. The ATR-FTIR spectra of the treated samples with Fe_3O_4 NPs/carbopol hybrid LV nanogel after aging (Fig. 20), observed the occurrence of C=O at 1677 cm^{-1}, CH at 1409 cm^{-1} and C–O–C at (991 cm^{-1}). By comparing the ATR-FTIR spectra of the treated samples before and after the aging process, the shifting of some functional groups was observed, which referred to the effect of the thermal aging process on the treated samples.

From the ATR-FTIR spectra of treated samples with Fe_3O_4 NPs/carbopol hybrid HV nanogel before aging (Fig. 20), the functional groups of OH (3230 cm^{-1}), CH (2856 cm^{-1}), C=O (1605 cm^{-1}) and OH (998 cm^{-1}) were characterized the cellulose structure. The characterized functional groups of mud almost disappeared. This led to the efficiency of this treatment compared to the treatment with the LV form of nanogel.

Moreover, the results of different microscopes confirmed the same obtained from ATR-FTIR analysis, where the spectra of the treated sample after aging (Fig. 20) revealed the presence of the same characteristic functional groups found in the ATR-FTIR spectra of the treated sample before aging, but with shifting to lower positions such as CH (shifted from 2856 to 2849 cm^{-1}) and C–O–C (shifted from 998 to 992 cm^{-1}).

By comparing the intensity of the vibrations characteristic of the paper before and after cleaning, we find an increase in the intensities of the vibrations at 3400 cm^{-1} (OH stretching) and groups of cellulose OH (3330 cm^{-1}) and OH starching (672 cm^{-1}) were increase after treatment, especially in high viscosity of Fe_3O_4 NPs/carbobol nanogel and ZnO NPs/carbopol hybrid nanogel furthermore the intensities of C=O at 1677 cm^{-1}, CH at 1409 cm^{-1} and C–O–C at (991 cm^{-1}) had been increased after treatment and it quickly declined under the influence of accelerated ageing. Furthermore, through Table 3, it can be noticed the disappearance of the CH vibration for treated samples with TiO_2 NPs/carbobol nanogel when comparing the sample before and after aging. One of the striking things is the increased intensity of the O–H stretching after treatment and aging by cleaning by TiO_2 NPs/carbobol nanogel and ZnO NPs/carbopol hybrid nanogel. Additionally, all visitations of ZnO NPs/carbopol hybrid nanogel such as OH starching (998 cm^{-1} or 3230 cm^{-1}), CH and C-O stretching (1050 cm^{-1}) have been observed, but all these peaks were slightly decreased after aging.

Conclusions

The treatment with ZnO NPs/carbopol hybrid nanogel at HV gave the best results in the cleaning process of mud stains. The results of the digital microscope showed that the treated paper sample with ZnO NPs/carbopol hybrid nanogel at HV gave the best results in removing dust stains without effect on the paper's fibers. The paper became white in some areas and the stain layer was removed. The roughness of the fibers and the tearing deformation of paper fibers were also noticed after the treatment by samples, but no noticeable differences were detected. Both treated paper's surface with TiO_2 NP/carbopol hybird HV nanogel after aging, ZnO NPs/carbopol hybrid HV nanogel after aging, and ZnO NPs/carbopol hybrid LV nanogel before aging are good results, but not as efficient as the previous materials. ZnO NPs/carbopol hybrid nanogel system gave the best results in most evaluation techniques used, where the aged treated sample with HV form of ZnO NPs/carbopol hybrid nanogel gave the highest tensile strength value of (56.0 N) and elongation (1.398%) before aging. Additionally, after washing the paper, it has no effect on its chemical composition. Instead, it hydrates the material overall, which improves the treated paper's qualities. The material treated with concentrated magnetite after aging gave the lowest tensile strength. It can be concluded the efficiency of ZnO NPs/carbopol hybrid LV nanogel with mud spots in the sample before aging is better than its efficiency after aging. The presence of residual impurities in both cases, but is found less in the treated sample before aging. Additionally, ZnO NPs/carbopol hybrid nanogel in the forms of HV and LV gave efficiency in cleaning stains on paper, but to varying degrees and not gave full efficiency in removing stains and impurities completely. There are residual impurities in each sample but in a small way. ZnO NPs/carbopol hybrid LV nanogel gave better results in the sample before aging. ZnO NPs/carbopol HV hybrid nanogel gave a better result in the sample after aging.

After the artificial aging, the values of ΔE in all treated samples declined dramatically, with the maximum value of 19.32 for the sample treated with ZnO NPs/Carbopol hybrid HV nanogel. The sample that was aged-treated with Fe_3O_4 NPs/carbopol hybrid LV nanogel had the lowest ΔE value (2.00). In conclusion, it was recommended to use ZnO NPs/carbopol hybrid nanogel in cleaning mud stains from paper manuscripts due to its satisfactory results compared to other treatments.

Acknowledgements
The authors would like to extent their appreciate to the scientific cooperation among the Department of Conservation, Faculty of Archaeology, Cairo University; Faculty of Nanotechnology for Post Graduates, Cairo University, El-Sheikh Zayed, and the Forestry and Wood Technology Department, Faculty of Agriculture (El-Shatby), Alexandria University.

Author contribution
RRAH, and MAH, wrote the main manuscript text, HMH, YAM, MEMI, YF, and HM prepared figures, SHI wrote the scientific methodology of the research, RRAH, MAH and MZM. Salem writing–review and editing, RRAH, and MA, MZMS, and SHI investigated the results. All authors perfectly reviewed the manuscript.

Funding
Open access funding provided by The Science, Technology & Innovation Funding Authority (STDF) in cooperation with The Egyptian Knowledge Bank (EKB).

Availability of data and materials
No data was used for the research described in the article.

Declarations

Competing interests
The authors declare no competing interests.

Received: 31 July 2023 Accepted: 30 September 2023
Published online: 18 October 2023

References

1. Salim E, Abdel-Hamied M, Salim S, Gamal S, Mohamed S, Galal F, et al. Reduction of borax / agar-based gel residues used to neutralize acidity of a historical manuscript with use of different paper barriers: artificial ageing results. BioResources. 2020;15(3):6576–99.
2. Abdel-Maksoud G. Analytical techniques used for the evaluation of a 19th century quranic manuscript conditions. Measurement. 2011;44(9):1606–17.
3. Strzelczyk AB. Observations on aesthetic and structural changes induced in polish historic objects by microorganisms. Int Biodeterior Biodegradation. 2004;53(3):151–6.
4. Sequeira S, Cabrita EJ, Macedo MF. Antifungals on paper conservation: an overview. Int Biodeterior Biodegrad. 2012;74:67–86.
5. Lloyd H, Bendix C, Brimblecombe P, Thickett D. Dust in historic libraries. Museum Microclim. 2007;52:135–44.
6. Wilson H, VanSnick S. The effectiveness of dust mitigation and cleaning strategies at the national archives. UK J Cultural Heritage. 2017;24:100–7.
7. Lloyd H, Grossi CM, Brimblecombe P. Low-technology dust monitoring for historic collections. J Inst Conserv. 2011;34(1):104–14.
8. Hassan RRA, Ali MF, Fahmy A-GA, Ali HM, Salem MZM. Documentation and evaluation of an ancient paper manuscript with leather binding using spectrometric methods. J Chem. 2020;2020:6847910.
9. Abdel-Maksoud G, Emam H, Ragab M. From traditional to laser cleaning techniques of parchment manuscripts: a review. Adv Res Conserv Sci. 2020;1(1):52–76.
10. García SJ, Fischer HR, van der Zwaag S. A critical appraisal of the potential of self healing polymeric coatings. Prog Org Coat. 2011;72(3):211–21.
11. Kim K. Conserving, Preserving, and Restoring Your Heritage: A Professional's Advice. Dundurn. 2010.
12. Pecht J. Long-term non-operating reliability of electronic products. Boca Raton: CRC Press; 2019.
13. Woko N, Feather J. Preservation and conservation problems of library materials in the tropical countries with special reference to Africa. Loughborough: Loughborough University of Technology; 1990.
14. Shahani CJ, Harrison G. Spontaneous formation of acids in the natural aging of paper. Stud Conserv. 2002;47(sup3):189–92.
15. Bras J, Viet D, Bruzzese C, Dufresne A. Correlation between stiffness of sheets prepared from cellulose whiskers and nanoparticles dimensions. Carbohyd Polym. 2011;84(1):211–5.
16. Strlic M, Kolar J. Ageing and stabilisation of paper. National and university library. 2005.
17. Theile Bruhns J, Guarda G, Croquevielle PE. Analysis, conservation and restoration of the metal threads used in Latin American colonial saints

robes. In: Ashton J, Hallam D, editors. Conservation Metal 2004. Canberra: National Museum of Australia Canberra ACT; 2004.
18. Gorassini A, Calvini P, Baldin A. Ourier transform infrared spectroscopy (FTIR) analysis of historic paper documents as a preliminary step for chemometrical analysis. In Italy: CMA4CH 2nd Mediterraneum meeting on multivariate analysis and chemometry for cultural heritage and environment 2008. 2 47–8
19. Mazzuca C, Micheli L, Carbone M, Basoli F, Cervelli E, Iannuccelli S, et al. Gellan hydrogel as a powerful tool in paper cleaning process: a detailed study. J Colloid Interface Sci. 2014;416:205–11.
20. Ferrari P, Chelazzi D, Bonelli N, Mirabile A, Giorgi R, Baglioni P. Alkyl carbonate solvents confined in poly (ethyl methacrylate) organogels for the removal of pressure sensitive tapes (PSTs) from contemporary drawings. J Cult Herit. 2018;34:227–36.
21. Koestler RJ, Santoro ED, Druzik J, Preusser F, Koepp L, Derrick M. Status report: ongoing studies of the susceptibility of stone consolidants to microbiologically induced deterioration. In: Houghton DR, Smith RN, Eggins HOW, editors. Biodeterioration 7. Dordrecht: Springer Netherlands; 1988. p. 441–8.
22. Florian M-L. Water, heritage photographic materials and fungi. Topics in photographic preservation. 2003. pp. 60–73.
23. Ochocińska K, Kamińska A, Śliwiński G. Experimental investigations of stained paper documents cleaned by the Nd:YAG laser pulses. J Cult Herit. 2003;4:188–93.
24. Abdel-Nasser M, Abdel-Maksoud G, Abdel-Aziz MS, Darwish SS, Hamed AA, Youssef AM. Evaluation of the efficiency of nanoparticles for increasing α-amylase enzyme activity for removing starch stain from paper artifacts. J Cult Herit. 2022;53:14–23.
25. Shaban NZ, Darouish SS, Salah TA. Experimental study on the cleaning of foxing spots on the old paper manuscripts using natural products. Int J Conserv Sci. 2016;7(4):1023–30.
26. Zornoza-Indart A, Lopez-Arce P. Silica nanoparticles (SiO_2): Influence of relative humidity in stone consolidation. J Cult Herit. 2016;18:258–70.
27. Zornoza-Indart A, Lopez-Arce P, Leal N, Simão J, Zoghlami K. Consolidation of a Tunisian bioclastic calcarenite: From conventional ethyl silicate products to nanostructured and nanoparticle based consolidants. Constr Build Mater. 2016;116:188–202.
28. Zidan Y, El-Shafei A, Noshy W, Salim E. A comparative study to evaluate conventional and nonconventional cleaning treatments of cellulosic paper supports. Mediter Archaeol Archaeom. 2017;17(3):337–53.
29. Usha SP, Mishra SK, Gupta BD. Fiber optic hydrogen sulfide gas sensors utilizing ZnO thin film/ZnO nanoparticles: a comparison of surface plasmon resonance and lossy mode resonance. Sens Actuators, B Chem. 2015;218:196–204.
30. Zafar MN, Dar Q, Nawaz F, Zafar MN, Iqbal M, Nazar MF. Effective adsorptive removal of azo dyes over spherical ZnO nanoparticles. J Market Res. 2019;8(1):713–25.
31. Mirzaeifard Z, Shariatinia Z, Jourshabani M, Rezaei Darvishi SM. ZnO photocatalyst revisited: effective photocatalytic degradation of emerging contaminants using S-doped ZnO nanoparticles under visible light radiation. Ind Eng Chem Res. 2020;59(36):15894–911.
32. Ullah R, Dutta J. Photocatalytic degradation of organic dyes with manganese-doped ZnO nanoparticles. J Hazard Mater. 2008;156(1):194–200.
33. Weldegebrieal GK. Synthesis method, antibacterial and photocatalytic activity of ZnO nanoparticles for azo dyes in wastewater treatment: a review. Inorg Chem Commun. 2020;120: 108140.
34. Mirzaei H, Darroudi M. Zinc oxide nanoparticlessynthesis and biomedical applications. Ceramics Int. 2017;43:907–14.
35. Asif N, Amir M, Fatma T. Recent advances in the synthesis, characterization and biomedical applications of zinc oxide nanoparticles. Bioprocess Biosyst Eng. 2023. https://doi.org/10.1007/s00449-023-02886-1.
36. Islam F, Shohag S, Uddin MJ, Islam MR, Nafady MH, Akter A, et al. Exploring the journey of zinc oxide nanoparticles (ZnO-NPs) toward biomedical applications. Materials. 2022;15(6):2160.
37. Wang M, Zhang M, Pang L, Yang C, Zhang Y, Hu J, et al. Fabrication of highly durable polysiloxane-zinc oxide (ZnO) coated polyethylene terephthalate (PET) fabric with improved ultraviolet resistance, hydrophobicity, and thermal resistance. J Colloid Interface Sci. 2019;537:91–100.
38. Radwan AB, Mohamed AMA, Abdullah AM, Al-Maadeed MA. Corrosion protection of electrospun PVDF–ZnO superhydrophobic coating. Surf Coat Technol. 2016;289:136–43.
39. Blinov AV, Kachanov MD, Gvozdenko AA, Nagdalian AA, Blinova AA, Rekhman ZA, et al. Synthesis and characterization of zinc oxide nanoparticles stabilized with biopolymers for application in wound-healing mixed gels. Gels. 2023;9(1):57.
40. Xu L, Liu Y, Yuan X, Wan J, Wang L, Pan H, et al. One-pot preparation of robust, ultraviolet-proof superhydrophobic cotton fabrics for self-cleaning and oil/water separation. Cellulose. 2020;27(15):9005–26.
41. Behera A. Self-Cleaning Materials. In: Behera A, editor. Advanced Materials: an introduction to modern materials science. Cham: Springer International Publishing; 2022. p. 359–94.
42. Jia M, Zhang X, Weng J, Zhang J, Zhang M. Protective coating of paper works: ZnO/cellulose nanocrystal composites and analytical characterization. J Cult Herit. 2019;38:64–74.
43. Fistos T, Fierascu I, Fierascu RC. Recent developments in the application of inorganic nanomaterials and nanosystems for the protection of cultural heritage organic artifacts. Nanomaterials. 2022;12(2):207.
44. Prasad V, Shaikh AJ, Kathe AA, Bisoyi DK, Verma AK, Vigneshwaran N. Functional behaviour of paper coated with zinc oxide–soluble starch nanocomposites. J Mater Process Technol. 2010;210(14):1962–7.
45. Julkapli NM, Bagheri S. Developments in nano-additives for paper industry. J Wood Sci. 2016;62(2):117–30.
46. Franco-Castillo I, Hierro L, de la Fuente JM, Seral-Ascaso A, Mitchell SG. Perspectives for antimicrobial nanomaterials in cultural heritage conservation. Chem. 2021;7(3):629–69.
47. Sungur Ş. Titanium Dioxide Nanoparticles. In: Kharissova O, Martínez L, Kharisov B, editors. Handbook of nanomaterials and nanocomposites for energy and environmental applications. Springer: Cham; 2021. p. 713–30.
48. Alejo-Molina E, Vilchis-Néstor AR, Muñoz-Rodríguez D, Carrera-Figueiras C. Synthesis and characterization of TiO_2 modified with polystyrene and Poly(3-chloro-2-hydroxypropyl Methacrylate) as adsorbents for the solid phase extraction of organophosphorus pesticides. J Chem. 2016;2016:1289592.
49. Blinov AV, Nagdalian AA, Arefeva LP, Varavka VN, Kudryakov OV, Gvozdenko AA, et al. Nanoscale composite protective preparation for cars paint and varnish coatings. Coatings. 2022;12(9):1267.
50. Irshad MA, Nawaz R, Rehman MZu, Adrees M, Rizwan M, Ali S, et al. Synthesis, characterization and advanced sustainable applications of titanium dioxide nanoparticles: a review. Ecotoxicol Environ Safety. 2021;212:111978.
51. Punia P, Bharti MK, Chalia S, Dhar R, Ravelo B, Thakur P, et al. Recent advances in synthesis, characterization, and applications of nanoparticles for contaminated water treatment—a review. Ceram Int. 2021;47(2):1526–50.
52. Li J, Shi X, Shen M. Hydrothermal synthesis and functionalization of iron oxide nanoparticles for mr imaging applications. Part Part Syst Charact. 2014;31(12):1223–37.
53. Hu Y, Mignani S, Majoral J-P, Shen M, Shi X. Construction of iron oxide nanoparticle-based hybrid platforms for tumor imaging and therapy. Chem Soc Rev. 2018;47(5):1874–900.
54. Lesiak B, Rangam N, Jiricek P, Gordeev I, Tóth J, Kövér L, et al. Surface study of Fe_3O_4 nanoparticles functionalized with biocompatible adsorbed molecules. Front Chem. 2019;7:642.
55. Ahmad W, Kumar Jaiswal K, Amjad M. *Euphorbia herita* leaf extract as a reducing agent in a facile green synthesis of iron oxide nanoparticles and antimicrobial activity evaluation. Inorgan Nano-Metal Chem. 2021;51(9):1147–54.
56. Biswas A, Vanlalveni C, Lalfakzuala R, Nath S, Rokhum SL. *Mikania mikrantha* leaf extract mediated biogenic synthesis of magnetic iron oxide nanoparticles: Characterization and its antimicrobial activity study. Mater Today Proc. 2021;42:1366–73.
57. Elnaggar A, Fitzsimons P, Lama A, Fletcher Y, Antunes P, Watkins KG. Feasibility of ultrafast picosecond laser cleaning of soiling on historical leather buckles. Heritage Sci. 2016;4(1):30.
58. Ismail SH, Hamdy A, Ismail TA, Mahboub HH, Mahmoud WH, Daoush WM. Synthesis and characterization of antibacterial carbopol/ZnO hybrid nanoparticles gel. Crystals. 2021;11(9):1092.
59. Gharib A, Maher MA, Ismail SH, Mohamed GG. Effect titanium dioxide/paraloid B 72 nanocomposite coating on protection of treated Cu-Zn archaeological alloys. Int J Archaeol. 2019;7(2):47–53.
60. Hamdy A, Ismail SH, Ebnalwaled AA, Mohamed GG. Characterization of superparamagnetic/monodisperse PEG-coated magnetite nanoparticles

sonochemically prepared from the hematite ore for Cd(II) removal from aqueous solutions. J Inorg Organomet Polym Mater. 2021;31(1):397–414.
61. El-Feky OM, Hassan EA, Fadel SM, Hassan ML. Use of ZnO nanoparticles for protecting oil paintings on paper support against dirt, fungal attack, and UV aging. J Cult Herit. 2014;15(2):165–72.
62. Bader NAAE-T, Ashry AM. The cleaning of the isis temple's mural paintings in upper Egypt using zinc oxide nanoparticles and non-ionic detergent. Int J Conserv Sci. 2016;7(2):443–58.
63. Ardelean E, Bobu E, Niculescu G, Groza C. Effects of different consolidation additives on ageing behaviour of archived document paper. Cellul Chem Technol. 2011;45(1–2):97–103.
64. Hassan RRA. Behavior of archeological paper after cleaning by organic solvents under heat accelerated ageing. Mediter Archaeol Archaeom. 2015;15(3):141–50.
65. Khalaf MK, Roshdy Elsakhry A, Ismail SH, Abdel-Hamied M, Mohamed GG. Evaluation of nanolime-silica core-shell for consolidation of egyptian limestone samples with application on an archaeological object nano hybrids and composites. Trans Tech Publ. 2022;37(91):102.
66. Abdel-Hamied M, Hassan RRA, Salem MZM, Ashraf T, Mohammed M, Mahmoud N, et al. Potential effects of nano-cellulose and nano-silica/polyvinyl alcohol nanocomposites in the strengthening of dyed paper manuscripts with madder: an experimental study. Sci Rep. 2022;12(1):19617.
67. Hassan RRA, Mahmoud SMA, Nessem MA, Aty RTA, Ramzy MG, Dessoky ES, et al. Hydroxypropyl cellulose loaded with ZnO nanoparticles for enhancing the mechanical properties of papyrus (*Cyperus papyrus* L) strips. BioResources. 2021;16(2):2607–25.
68. Abdel-Maksoud G, Abdel-Hamied M, Abdelhafez AAM. Evaluation of the condition of a Mamluk-illuminated paper manuscript at Al-Azhar Library. Egypt Pigment Resin Technol. 2023;52(1):49–59.
69. ISO-187. Paper, board and pulps—Standard atmosphere for conditioning and testing and procedure for monitoring the atmosphere and conditioning of samples. Geneva: International Organization for Standardization; 1990.
70. Abdel-Maksoud G, El-Shemy H, Abdel-Hamied M. Investigation methods for evaluating the preservative organic mixtures applied on a Late Period mummy. Archaeol Anthropol Sci. 2019;11(5):1843–50.
71. Rajeevgandhi C, Bharanidharan S, Savithiri S, Guganathan L, Sugumar P, Sathiyamurthy K, et al. Synthesis, characterizations and quantum chemical calculations of the spinel structure of Fe_3O_4 nanoparticles. J Mater Sci: Mater Electron. 2020;31(23):21419–30.
72. Zeng S, Gan N, Weideman-Mera R, Cao Y, Li T, Sang W. Enrichment of polychlorinated biphenyl 28 from aqueous solutions using Fe_3O_4 grafted graphene oxide. Chem Eng J. 2013;218:108–15.
73. Recillas S, García A, González E, Casals E, Puntes V, Sánchez A, et al. Use of CeO_2, TiO_2 and Fe_3O_4 nanoparticles for the removal of lead from water: toxicity of nanoparticles and derived compounds. Desalination. 2011;277(1):213–20.
74. Taheri-Ledari R, Valadi K, Gharibi S, Maleki A. Synergistic photocatalytic effect between green LED light and Fe_3O_4/ZnO-modified natural pumice: a novel cleaner product for degradation of methylene blue. Mater Res Bull. 2020;130: 110946.
75. Chang M, Lin Y-H, Gabayno JL, Li Q, Liu X. Thrombolysis based on magnetically-controlled surface-functionalized Fe_3O_4 nanoparticle. Bioengineered. 2017;8(1):29–35.
76. Bai X, Liu P, Gao X, Liu K, Li A, Lyu Z, et al. The Fe3O4@UiO-66-NH_2/PVDF-co-CTFE mixed matrix membrane with enhanced anti-fouling and self-cleaning performances for effectively removing dyes by Fenton reaction. Mater Chem Phys. 2023;301: 127657.
77. Farr JP, Smith WL. Steichen DS bleaching agents. Kirk-Othmer Encyclopedia of chemical technology. Hoboken: Wiley; 2003.
78. Osman E, Ibrahim S, Michael M. Characterization of artificially dyed aged stained cotton carpets to simulate the archeological model samples. Elixir Int J Chem Phys Lett. 2011;35:2777–82.
79. Md Salim R, Asik J, Sarjadi MS. Chemical functional groups of extractives, cellulose and lignin extracted from native *Leucaena leucocephala* bark. Wood Sci Technol. 2021;55(2):295–313.
80. Nogales-Bueno J, Baca-Bocanegra B, Rooney A, Miguel Hernández-Hierro J, José Heredia F, Byrne HJ. Linking ATR-FTIR and Raman features to phenolic extractability and other attributes in grape skin. Talanta. 2017;167:44–50.
81. Hospodarova V, Singovszka E, Stevulova N. Characterization of cellulosic fibers by FTIR spectroscopy for their further implementation to building materials. Am J Anal Chem. 2018;9(6):303–10.

Publisher's Note